Research Square

Preprints are preliminary reports that have not undergone peer review.
They should not be considered conclusive, used to inform clinical practice,
or referenced by the media as validated information.

Spectral origin and decoupling cost of non-Markovian ergotropy revivals in quantum batteries

Hikaru Wakaura

hikaruwakaura@gmail.com

QuantScape Inc

Research Article

Keywords: quantum battery , ergotropy , system--bath binding

Posted Date: November 2nd, 2026

DOI: https://doi.org/10.21203/rs.3.rs-11546136/v1

License: This work is licensed under a Creative Commons Attribution 4.0 International License.
Read Full License

Additional Declarations: The authors declare no competing interests.

Spectral origin and decoupling cost of non-Markovian ergotropy revivals in quantum batteries

Hikaru Wakaura[1, *]

[1] *QIRI (Quantum Integrated Research Institute Inc.), Tokyo 107-0061, Japan*

(Dated: October 26, 2026)

Because every quantum battery is an open system, environmental memory (non-Markovianity) has been widely proposed to revive the extractable work, or ergotropy, that dissipation destroys. These predictions rest on rotating-wave, zero-temperature or second-order treatments and evaluate the ergotropy of a still-coupled battery, leaving open whether the revival is physical and how much of it can be withdrawn. We address both questions with numerically exact hierarchical equations of motion, extended to time-dependent system–bath coupling, for single and collective qubit batteries in structured baths. The revival is physical but stems from spectral weight at the battery frequency, not from memory: baths with long memory but no such weight store less work than a Markovian bath. Disconnecting the battery costs work, which we obtain in closed form. In second-order theory a revival yields net work only if it exceeds the system–bath binding energy, a bound that a smooth coupling ramp lasting a few battery periods nearly reaches, whereas a fast local unitary avoids disconnection. In circuit quantum electrodynamics, these predictions are testable with 0.2–1 ns coupling ramps and qubit readout alone. The figure of merit of an open quantum battery is therefore set by how its energy is withdrawn.

I. INTRODUCTION

Every quantum technology runs on energy that is prepared, stored and released at the level of individual quantum systems. Quantum batteries make this explicit: they store energy in quantum degrees of freedom and quantify its usable part by the ergotropy, the maximum work that a cyclic unitary process can extract [1]. Entangling and collective operations can speed up charging beyond what independent cells allow [2–4], and the field has grown into a broad theoretical program [5, 6] with first demonstrations on superconducting processors [7, 8], trapped ions [9], organic microcavities [10], photonic platforms [11] and spin defects [12].

No battery is isolated. Its environment drives the stored state towards a passive one, from which no work can be extracted, and this self-discharging is the central obstacle to practical devices [5, 13]. A large and growing literature has argued that the remedy lies in the environment itself: when the bath retains memory of the battery, information and energy flow back, the ergotropy revives, and both charging and storage improve over the Markovian limit [14–20]. The same mechanism has been invoked to charge batteries wirelessly through a shared structured bath [16, 21, 22], to protect energy in dark and bound states [22, 23], and to produce anomalous, Mpemba-like discharging [24, 25]. Separating the ergotropy into coherent and incoherent parts [26] has made these memory effects visible in experiments [8, 11].

The theoretical evidence for this non-Markovian advantage rests on three kinds of treatment. Exact single-excitation solutions for Lorentzian baths within the rotating-wave approximation [27, 28] underlie many of the charging and storage studies [14, 16]; they are restricted to zero temperature and to energy-conserving coupling. Regimes labelled as strong coupling are typically treated with Redfield or memory-kernel master equations [29–32], which truncate the system–bath interaction at second order. And in nearly all of these studies the ergotropy is evaluated for the reduced state of a battery that is still coupled to its environment, although the work that can be extracted from a coupled system is known to depend on whether, and how, the coupling is switched off first [33–35]. Strong-coupling thermodynamics has shown that this last step is not innocent. The interaction energy is part of the work budget, a battery can be charged by thermalization alone [36], and for a harmonic battery charged in this way the numerically computed work to disconnect and reconnect it bounds the efficiency of the cycle [37]. The equilibrium state of a strongly coupled system is described by a Hamiltonian of mean force [38–41], whose identification with a local energy and temperature is itself ambiguous [42, 43]. Numerically exact methods that capture all of these effects—hierarchical equations of motion (HEOM) [44–46], reaction-coordinate mappings [47–49], pseudomodes [50, 51] and process tensors [52, 53]—are now routinely used for strong-coupling thermodynamics [54], yet they have not been brought to bear on the ergotropy of batteries, and only recently has it been suggested that memory may not be needed at all [55].

However, because the existing treatments truncate the system–bath interaction or omit the work needed to disconnect the battery, it cannot be decided whether the non-Markovian gain is physical or an artifact of approximation, whether it stems from memory or from the spectral structure of the bath, and how much of it can be withdrawn as work. In this study, we answer these questions with numerically exact HEOM, extended to a time-dependent system–bath coupling and cross-

* h.wakaura@qiri.co.jp

checked by reaction-coordinate dynamics, for three representative protocols—storage, charger-mediated charging and charging through a shared bath [Fig. 1(a)]—for underdamped, detuned, overdamped (Drude–Lorentz) and Ohmic spectral densities, and for collective batteries of up to three cells. We develop a closed-form theory of the work required to decouple a qubit battery that applies to dynamical revivals and yields the finite-time decoupling ramp. We found that the work required to disconnect the battery, the decoupling toll, obeys a closed form set by the counter-rotating binding energy, a resonant thermal term and a static polaron term, whereas ergotropy referred to the Hamiltonian of mean force collapses at low temperature (Sec. V). We found that, in second-order theory, a revival yields net work after disconnection only if it exceeds the system–bath binding energy, which is half the toll of sudden decoupling, that a $\cos^2$ ramp lasting a few battery periods reaches this bound [Fig. 1(c)], that a fast local unitary extracts the revival in place without paying the toll, and that in collective batteries the toll per cell exceeds its second-order value (Sec. VI). The result shows that the ergotropy of the coupled battery measures the work available in place but overestimates the work available after disconnection, and that the latter can be predicted and optimized analytically. These predictions rest on two findings about the gain itself. We found that the rotating-wave, zero-temperature and Redfield treatments on which the reported gains rest fail in sharply identifiable regions: at $T = 0.1\,\omega_0$ the rotating-wave solution overestimates the peak ergotropy delivered through a shared bath by a factor of 27.5 (the delivered energy by 33%), zero-temperature solutions overestimate stored work at $T = \omega_0$ by factors of 2.6–3.2, and the Redfield equation overestimates the peak ergotropy delivered by a charger by a factor of 43.5 (the delivered energy by 69%; Fig. 2). We found that, where the gain is physical, it requires spectral weight at the battery frequency and that non-Markovianity, measured by information backflow, does not predict it: baths with long memory and strong information backflow but without such weight degrade the battery faster than a Markovian bath (Fig. 3).

These findings turn the non-Markovian advantage from a qualitative expectation into a quantitative design rule. They identify which reported gains survive exact dynamics and finite temperature—for superconducting circuits operating at $T \approx 0.08\,\omega_0$, the rotating-wave predictions remain accurate for single-channel protocols but fail for shared baths at strong coupling—and they supply the coupling-ramp protocol that turns a revival into usable work. Because the toll and its finite-time optimum depend only on the system–bath correlation function, the same reasoning applies to any device that must be connected to and disconnected from a structured environment, from strongly coupled heat engines to quantum sensors and work buffers in error-corrected processors [56]. The paper is organized as follows. Section II introduces the models and methods, Sec. III maps the validity of standard treatments, Sec. IV identifies the origin of the gain, Sec. V derives the decoupling toll, Sec. VI establishes the harvesting criterion and the decoupling ramp, Sec. VII maps the results onto circuit quantum electrodynamics and proposes experimental tests, and Sec. VIII discusses implications and limits.

II. MODELS AND METHODS

A. Batteries, protocols and baths

We consider a qubit battery B with Hamiltonian $H_B = \frac{\omega_0}{2}\sigma_z^B$ and, where needed, a qubit charger C with the same splitting. The system Hamiltonian H_S and the operator Q through which the system couples to a bosonic environment define three protocols that cover the settings studied in the literature:

- *storage*: $H_S = H_B$ and $Q = \cos\varphi\,\sigma_x^B + \sin\varphi\,\sigma_z^B$, with the battery initially in $|\psi\rangle = \cos\frac{\theta}{2}|e\rangle + \sin\frac{\theta}{2}|g\rangle$ and $\theta = \pi/3$, so that both population inversion and coherence contribute to the ergotropy;
- *charger-mediated charging*: $H_S = \frac{\omega_0}{2}(\sigma_z^C + \sigma_z^B) + g(\sigma_+^C\sigma_-^B + \text{h.c.})$ with $g = 0.1\,\omega_0$, $Q = \sigma_x^C$, and initial state $|e\rangle_C|g\rangle_B$;
- *shared-bath charging*: $H_S = \frac{\omega_0}{2}(\sigma_z^C + \sigma_z^B)$ without direct coupling, $Q = \sigma_x^C + \sigma_x^B$, and initial state $|e\rangle_C|g\rangle_B$, so that energy can reach the battery only through the common environment.

Unless stated otherwise $\varphi = 0$, i.e., the parity-symmetric coupling used throughout the battery literature; the tilted case $\varphi \neq 0$ is analysed in Sec. V.

The total Hamiltonian is

$$H = H_S + Q \otimes X + H_E, \tag{1}$$

with $X = \sum_k c_k(b_k + b_k^\dagger)$ and $H_E = \sum_k \omega_k b_k^\dagger b_k$, the environment being initially in a Gibbs state at temperature $T = 1/\beta$ and uncorrelated with the system, so that the coupling is switched on suddenly at $t = 0$, as in the literature. All environmental effects are encoded in the correlation function

$$\begin{aligned} C(t) &= \langle X(t)X(0)\rangle \\ &= \frac{1}{\pi}\int_0^\infty d\omega\, J(\omega)\Big[\coth\frac{\beta\omega}{2}\cos\omega t - i\sin\omega t\Big], \end{aligned} \tag{2}$$

where $J(\omega) = \pi\sum_k c_k^2\delta(\omega - \omega_k)$ is the spectral density. We use three families. The *underdamped* (Brownian) density

$$J_{\rm UD}(\omega) = \frac{\lambda^2\Gamma\,\omega}{(\omega_r^2 - \omega^2)^2 + \Gamma^2\omega^2} \tag{3}$$

has a peak of width Γ at ω_r, which we place on resonance, $\omega_r = \omega_0$. It is exactly equivalent to a single bosonic mode a—the reaction coordinate (RC)—coupled to the

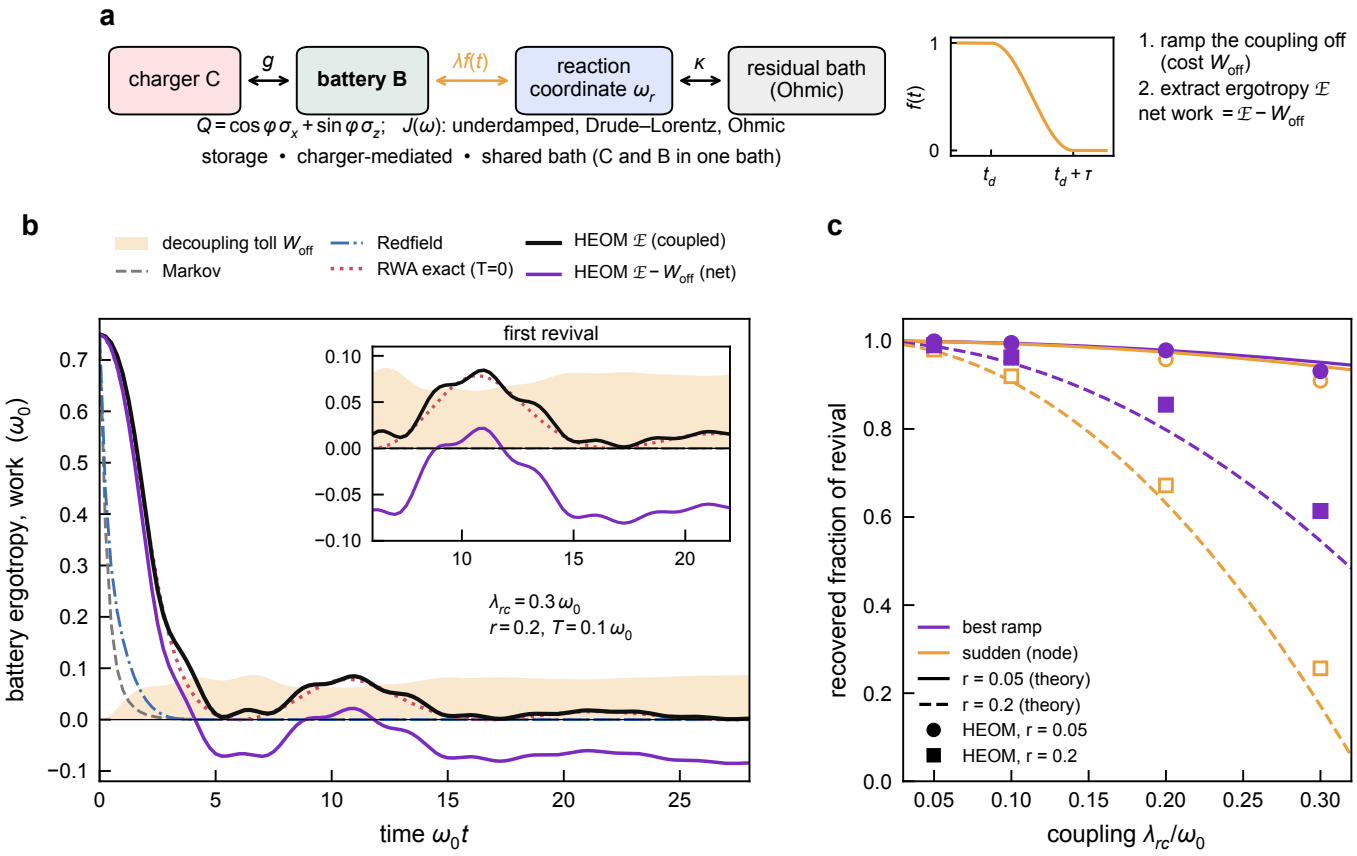


FIG. 1. **Non-Markovian ergotropy revivals are real but are largely consumed by the work needed to decouple the battery.** (a) Battery B coupled through $Q = \cos\varphi\,\sigma_x + \sin\varphi\,\sigma_z$ to a structured bath, represented exactly as a reaction coordinate damped by an Ohmic residual bath; a charger C enters the charger-mediated and shared-bath protocols. Work is withdrawn by switching the coupling off with $f(t)$ and then extracting the ergotropy. (b) HEOM ergotropy of the coupled battery (black), the instantaneous decoupling toll $W_{\rm off} = -\langle H_I\rangle$ (shaded) and their difference (purple) for $\lambda_{rc} = 0.3\,\omega_0$, $r = 0.2$, $T = 0.1\,\omega_0$, $\varphi = 0$, compared with Markovian, Redfield and zero-temperature rotating-wave predictions. Inset: first revival. (c) Fraction of the first revival recovered as net work for sudden decoupling at a counter-rotating node and for the best $\cos^2$ ramp. Lines: Eq. (19); symbols: HEOM with a time-dependent coupling.

system as $\lambda_{rc}Q(a+a^\dagger)$ and damped by an Ohmic residual bath [47, 48], with

$$\lambda_{rc}^2 = \frac{\lambda^2}{2\omega_r}, \qquad \kappa = \Gamma. \tag{4}$$

In the narrow-peak limit $J_{\rm UD}$ reduces to the Lorentzian of width $\kappa/2$ and golden-rule decay rate $\gamma_0 = 4\lambda_{rc}^2/\kappa$ used in the literature [27, 28]. The literature criterion for non-Markovian dynamics, width $< 2\gamma_0$, then reads

$$r \equiv \frac{\kappa}{4\lambda_{rc}} < 1, \tag{5}$$

and we use (λ_{rc}, r) as the two control parameters. We also consider the overdamped Drude–Lorentz density $J_{\rm DL}(\omega) = 2\lambda_{\rm DL}\gamma\omega/(\omega^2+\gamma^2)$, whose memory time $1/\gamma$ can be long without any spectral weight near ω_0, and the Ohmic density $J_{\rm O}(\omega) = \alpha\,\omega\,e^{-\omega/\omega_c}$. As a control we also detune the underdamped peak, $\omega_r \neq \omega_0$ at fixed κ, which keeps the memory time but removes the weight at ω_0.

We set $\omega_0 = 1$ and scan $\lambda_{rc} \in \{0.02, 0.05, 0.1, 0.2, 0.3\}$, $r \in \{0.05, 0.2, 1, 5\}$ and $T \in \{0.1, 0.5, 1\}$; for Drude–Lorentz and Ohmic baths, $\lambda_{\rm DL} \in \{0.01, 0.03, 0.1\}$, $\gamma \in \{0.05, 0.2, 1, 5\}$, $\alpha \in \{0.01, 0.05\}$ and $\omega_c \in \{1, 5\}$. Superconducting circuits typically operate near $T \approx 0.08\,\omega_0$, close to the lowest temperature considered.

B. Numerically exact dynamics

Our reference is the HEOM [44, 45], as implemented in QuTiP-BoFiN [46]. The correlation function (2) is expanded in exponentials: Matsubara terms for underdamped baths ($N_k = 3$), Padé terms for Drude–Lorentz baths ($N_k = 3$–6), and least-squares fits with two to four exponentials of $C(t)$ itself for overdamped Brownian baths ($\Gamma \geq 2\omega_r$, where the analytic Matsubara decomposition does not apply) and for Ohmic baths. The hierarchy is truncated at depth 5–16. We accept a result when increasing N_k or the depth changes the fig-

ure of merit by less than 1%. Appendix A documents these tests. It identifies the regimes in which the default depth is insufficient—shared-bath charging at strong coupling or high temperature, slow Drude–Lorentz baths at $T = 0.5\,\omega_0$, and the overdamped bath at $T = \omega_0$—for which we use values from deeper hierarchies, and two parameter sets in which the hierarchy is numerically unstable and which we exclude (shared-bath charging at $\lambda_{rc} = 0.3$, $r = 0.05$, $T = 0.1\,\omega_0$, and all Drude–Lorentz runs with $\gamma = 5\,\omega_0$ at $T = 0.1\,\omega_0$).

As an independent check we integrate the RC model,

$$\begin{aligned}\dot\rho = &-i\big[H_S + \omega_r a^\dagger a + \lambda_{rc} Q(a + a^\dagger), \rho\big] \\ &+ \kappa(\bar n + 1)\mathcal{D}[a]\rho + \kappa\bar n\,\mathcal{D}[a^\dagger]\rho, \end{aligned} \tag{6}$$

with $\mathcal{D}[L]\rho = L\rho L^\dagger - \frac{1}{2}\{L^\dagger L, \rho\}$, $\bar n = (e^{\beta\omega_r} - 1)^{-1}$ and a Fock-space cutoff of 14 (converged against 24, Appendix A). Across all points with $T \le 0.5$ and $r \le 1$, the RC and HEOM figures of merit differ by 0.2% in the median, and by less than 4% for 58 of 65 points (Appendix A). Finite-time decoupling (Sec. VI) is computed with HEOM directly. The HEOM generator is linear in the coupling operator, so a time-dependent coupling $f(t)Q$ gives $\mathcal{L}(t) = \mathcal{L}_0 + f(t)\mathcal{L}_1$, where both parts are obtained exactly from the hierarchies built for Q and $2Q$; the bath correlation function is unchanged. The ramp work $W = \int dt\, \dot f(t)\langle H_I\rangle(t)$ then follows from the first-tier auxiliary density operators (Appendix A).

C. Treatments under test

We compare three treatments that underlie the claims tested here, all built on the same $J(\omega)$. (i) *Rotating-wave exact solution*: Eq. (6) with $Q(a + a^\dagger)$ replaced by $\sigma_+ a + \sigma_- a^\dagger$ (summed over C and B for the shared bath), at $T = 0$. Because the excitation number is conserved, this is identical to the exact single-excitation solution for a Lorentzian bath [14, 16, 27, 28]. (ii) *Bloch–Redfield*: the non-secular second-order master equation with the full power spectrum $S(\omega) = 2J(\omega)[\bar n(\omega)+1]$ [29–31]. (iii) *Golden-rule (Markovian) master equation*: a Lindblad equation with rates $2J(\omega_0)(\bar n+1)$ and $2J(\omega_0)\bar n$, acting locally on the coupled qubit (collectively, through $\sigma_-^C + \sigma_-^B$, for the shared bath). This is the Markovian reference against which non-Markovian gains are usually measured.

D. Figures of merit

The ergotropy of the battery state ρ_B is

$$\mathcal{E}(\rho_B) = \mathrm{Tr}[\rho_B H_B] - \mathrm{Tr}[\pi_{\rho_B} H_B], \tag{7}$$

where the passive state π_{ρ_B} has the eigenvalues of ρ_B ordered inversely to the energies [1]. It splits into an incoherent part $\mathcal{E}_i$, the ergotropy of ρ_B dephased in the eigenbasis of H_B, and a coherent part $\mathcal{E}_c = \mathcal{E} - \mathcal{E}_i$ [26]. For storage we use the time-integrated ergotropy $\int_0^{t_f} \mathcal{E}\,dt$, with $t_f = \min[\max(8/\kappa, 60), 600]/\omega_0$ so that the window always contains the revivals; for charging we use the peak battery ergotropy $\max_t \mathcal{E}_B(t)$. Equation (7) is the quantity reported in the literature: the ergotropy of the battery while it is still coupled to the bath. In Secs. V and VI we complement it with the work needed to decouple the battery,

$$W_{\mathrm{off}}(t) = -\langle H_I\rangle(t), \qquad \langle H_I\rangle = \sum_k \mathrm{Tr}\big[Q\,\rho^{(k)}\big], \tag{8}$$

where the sum runs over the first-tier auxiliary density operators $\rho^{(k)}$ of the hierarchy. In equilibrium this expression reproduces the interaction energy $\lambda_{rc}\langle Q(a+a^\dagger)\rangle$ of the system–RC Gibbs state to within 0.4% (Appendix A).

III. VALIDITY OF STANDARD TREATMENTS

Figure 2 compares the three treatments with HEOM over the full parameter grid. The comparison separates three questions: whether the rotating-wave single-excitation solutions are reliable, whether zero-temperature results transfer to finite temperature, and whether second-order master equations can describe the regimes labelled as strong coupling.

A. Rotating-wave solutions: accurate for single channels, unreliable for shared baths

For storage and for charger-mediated charging, the rotating-wave solution is quantitatively reliable at low temperature [Fig. 2(a), left and middle]. At $T = 0.1\,\omega_0$ and throughout the non-Markovian regime $r < 1$, its figure of merit lies between 0.92 and 1.00 times the exact value for both protocols. The residual deviation grows with coupling, because the counter-rotating terms neglected by the rotating-wave approximation shift and dress the battery levels by an amount of order λ_{rc}^2/ω_0. Within this domain the qualitative conclusions of Ref. [14]—that memory revives the stored ergotropy and enables charging where the Markovian limit gives none—are confirmed by the exact dynamics.

Charging through a shared bath is different [Fig. 2(a), right]. The rotating-wave solution overestimates the peak battery ergotropy by 7–11% at $\lambda_{rc} = 0.1$, by 32–67% at $\lambda_{rc} = 0.2$, and by a factor of 27.5 at $\lambda_{rc} = 0.3$, $r = 0.2$, where it predicts $\mathcal{E}_B = 0.342\,\omega_0$ while the converged HEOM gives $0.0124\,\omega_0$ [Fig. 2(d)]. Because the battery state is diagonal in these protocols, its ergotropy $\omega_0 \max(0, 2p_e - 1)$ has a threshold at $p_e = 1/2$, and large factors arise where the exact dynamics barely crosses it: the excited-state populations are 0.671 and 0.506, so the delivered energy is overestimated by 33%,

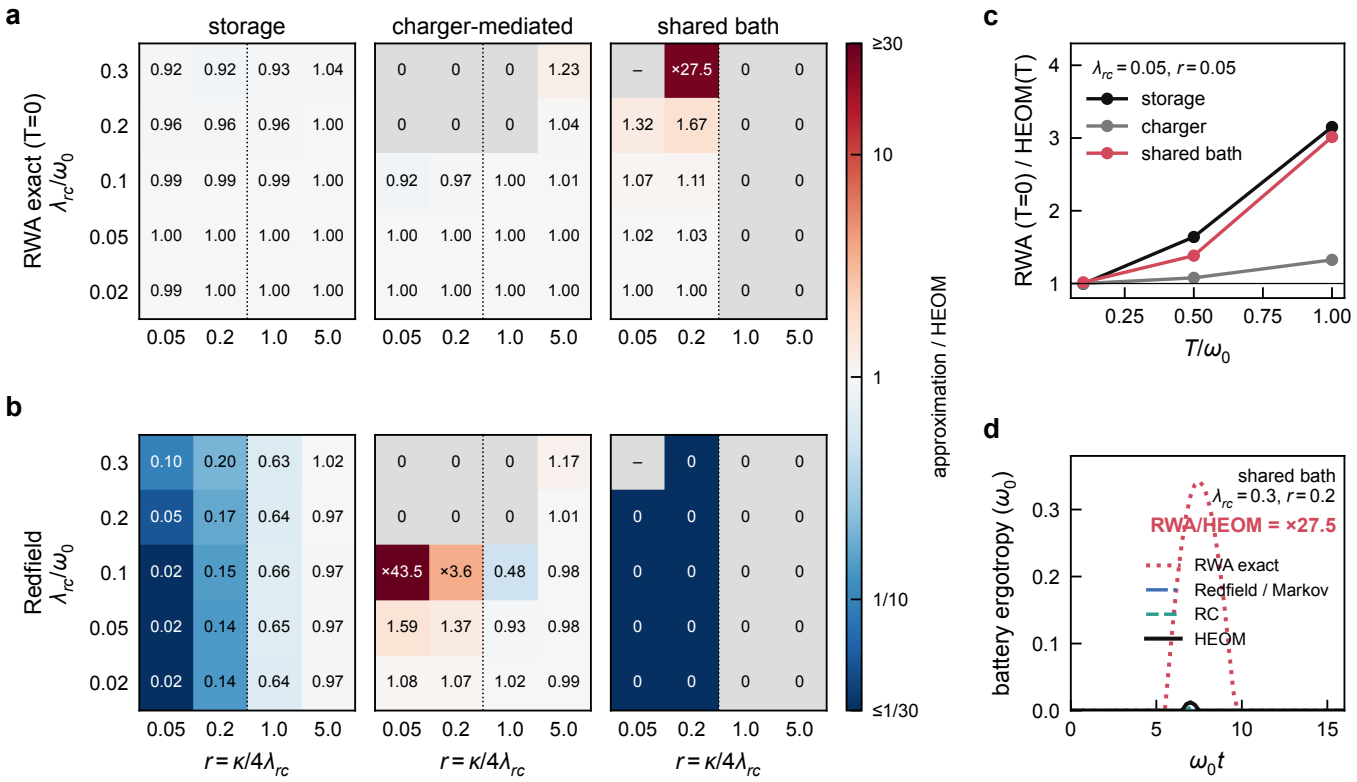


FIG. 2. **Standard treatments of open quantum batteries fail in identifiable regions.** Ratio of the approximate to the exact (HEOM) figure of merit at $T = 0.1\,\omega_0$ (storage: time-integrated ergotropy; charging protocols: peak battery ergotropy) for (a) the zero-temperature rotating-wave single-excitation solution and (b) the Bloch–Redfield equation, as a function of coupling λ_{rc} and $r = \kappa/4\lambda_{rc}$. Dotted lines mark the non-Markovian threshold $r = 1$ of Eq. (5). "0": both vanish; "∞": the approximation predicts charging that the exact dynamics does not deliver; "–": no converged reference. (c) Overestimate by zero-temperature rotating-wave solutions applied at finite temperature ($\lambda_{rc} = 0.05$, $r = 0.05$). (d) Shared-bath charging at $\lambda_{rc} = 0.3$, $r = 0.2$: the rotating-wave solution predicts a peak battery ergotropy 27.5 times larger than the exact dynamics delivers, while Redfield and Markovian equations predict none.

whereas the extractable work is overestimated 27.5-fold. The reason is not a breakdown of dark-state protection. The antisymmetric state $|S\rangle = (|eg\rangle - |ge\rangle)/\sqrt{2}$ satisfies $Q|S\rangle = 0$ for $Q = \sigma_x^C + \sigma_x^B$ and therefore remains exactly dark, counter-rotating terms included. Transfer from C to B requires instead that the bright component $|T_0\rangle = (|eg\rangle + |ge\rangle)/\sqrt{2}$ of the initial state $|eg\rangle = (|T_0\rangle + |S\rangle)/\sqrt{2}$ acquire a phase π relative to $|S\rangle$. The bright state couples to the bath with the collective strength $\sqrt{2}\lambda_{rc}$, so the counter-rotating terms shift its frequency and leak its amplitude into $|gg\rangle$ and $|ee\rangle$, which destroys the phase condition on which charging relies. Dark-state trapping of energy in a shared bath [22, 23] therefore survives in the exact dynamics, whereas the charging peak predicted for strong collective coupling [16, 21, 22] does not survive once $\lambda_{rc}/\omega_0 \gtrsim 0.2$. In Ref. [16] strong coupling refers to the ratio of the Rabi frequency to the bath width, i.e. $r < 1$; in that sense, and for $\lambda_{rc} \lesssim 0.1\,\omega_0$, the rotating-wave prediction is confirmed to within 11%.

B. Zero-temperature solutions at finite temperature

Most non-Markovian battery solutions assume a vacuum environment. Figure 2(c) shows what happens when they are used to describe a device at finite temperature. At $T = 0.5\,\omega_0$ the zero-temperature result overestimates the exact figure of merit by factors of 1.64 (storage), 1.08 (charger-mediated) and 1.38 (shared bath); at $T = \omega_0$ the factors grow to 3.15, 1.32 and 3.0 ($\lambda_{rc} = 0.05$, $r = 0.05$; for $\lambda_{rc} = 0.02$ the storage factor is 2.6). Thermal photons in the structured bath randomize the phases of the vacuum Rabi oscillation that produces the revival, and photons absorbed from the bath during the revival degrade it further; Sec. VI turns this into a quantitative theory. The non-Markovian gain survives these losses as a ratio—at $T = \omega_0$ the exact storage figure of merit still exceeds the Markovian one by a factor of about 40 for $\lambda_{rc} = 0.02$—but its absolute size is about three times smaller than zero-temperature solutions suggest. For superconducting circuits at $T \approx 0.08\,\omega_0$ the correction is negligible; for spin-based and other low-frequency plat-

forms operated at $T \gtrsim \omega_0$ it is not.

C. The Bloch–Redfield equation in the non-Markovian regime

The Bloch–Redfield equation fails throughout the non-Markovian regime [Fig. 2(b)], and in a direction that depends on the protocol. For storage it underestimates the time-integrated ergotropy by 80–98.5% (ratios 0.015–0.20 for $r < 1$), because its time-independent rates cannot generate revivals. For charger-mediated charging it overestimates the peak battery ergotropy by up to a factor of 43.5 ($0.72\,\omega_0$ against $0.017\,\omega_0$ at $\lambda_{rc} = 0.1$, $r = 0.05$; excited-state populations 0.860 against 0.508, i.e. 69% in delivered energy). The next-largest factor on the grid is 3.6 ($r = 0.2$). Here the golden-rule rate $\gamma_0 = \lambda_{rc}/r$ exceeds both the charger–battery coupling g and the bath width, so the separation of time scales on which the second-order equation rests no longer exists. For shared-bath charging it predicts no charging at all, missing the coherent exchange mediated by the structured bath. Agreement is recovered only for broad baths ($r = 5$), where Redfield and HEOM agree to within 3.2% for storage and 17% for charger-mediated charging. Studies that use the Bloch–Redfield equation to describe strongly coupled, non-Markovian batteries [29–31] therefore rest on an approximation that is uncontrolled precisely in the regime of interest. For slow overdamped baths and tilted coupling ($\varphi = \pi/4$) it even violates positivity, with density-matrix eigenvalues down to -0.15 (Sec. IV).

The Markovian reference itself is reliable where it should be. For broad baths ($r = 5$) at $T = 0.1\,\omega_0$ it agrees with HEOM to within 3.2% for storage (and 19% for charger-mediated charging), so gains measured against it in Secs. IV–VI are meaningful. Strong coupling at high temperature is an exception even for broad baths. At $\lambda_{rc} = 0.3$ the golden-rule equation overestimates the stored ergotropy by 46% ($T = 0.5$) and 59% ($T = \omega_0$), and for charger-mediated charging at $T = 0.5$ it predicts a peak ergotropy of $0.235\,\omega_0$ where the exact dynamics never brings the battery past population inversion ($\mathcal{E}_B = 0$).

Taken together, Fig. 2 provides a validity map. The rotating-wave solutions remain accurate (to within 8.4%) for single-channel protocols at low temperature throughout the non-Markovian regime $r < 1$ up to $\lambda_{rc} = 0.3\,\omega_0$; they fail for shared-bath charging beyond $\lambda_{rc} \approx 0.1\,\omega_0$ and, as zero-temperature solutions, at $T \gtrsim 0.5\,\omega_0$. The time-independent Bloch–Redfield equation should not be used for $r < 1$; time-convolutionless and memory-kernel equations were not tested here. The non-Markovian advantage is therefore a physical effect, but its reported size depends on the treatment. Section IV asks what produces it.

IV. SPECTRAL ORIGIN OF THE NON-MARKOVIAN GAIN

The non-Markovian advantage is usually attributed to memory: a bath that remembers the battery returns information and energy to it [14, 15, 17, 18]. If memory produced the gain, the gain should track a measure of memory. Figure 3 tests this with two such measures, the bath memory time τ_B and the Breuer–Laine–Piilo non-Markovianity $\mathcal{N}_{\mathrm{BLP}}$ [57], the total increase of the trace distance between two evolving battery states. We evaluate it for the pairs $(|e\rangle, |g\rangle)$ and $(|+\rangle, |-\rangle)$, which gives a lower bound, and, where this bound vanishes, take the largest value over a sample of orthogonal pure-state pairs. In each case it measures the stored ergotropy relative to the golden-rule limit with the same rate $2J(\omega_0)$.

For underdamped baths, which carry their spectral weight in a peak at the battery frequency, the exact gain grows monotonically with memory time and reaches a factor of 82 ($\lambda_{rc} = 0.05$, $r = 0.05$, $T = 0.1$). Even at $r = 1$, the threshold of Eq. (5), it is 1.5–1.8. The gain decreases only moderately with temperature, from 82 to 57 at $T = 0.5\,\omega_0$ for the same parameters.

Drude–Lorentz baths behave in the opposite way. Their spectral weight is concentrated at frequencies of order $\gamma \ll \omega_0$, so a long memory time $1/\gamma$ comes with little weight at the battery frequency. For $\gamma = 0.05\,\omega_0$ ($\tau_B = 20/\omega_0$) the exact stored ergotropy falls below the Markovian value: to 0.74 of it at $T = 0.1$ and $\lambda_{\mathrm{DL}} = 0.1$, and to 0.45 at $T = 0.5$, where the deviation grows with both coupling (0.87, 0.60 and 0.45 for $\lambda_{\mathrm{DL}} = 0.01$, 0.03 and 0.1) and slowness of the bath (0.73 at $\gamma = 0.2$). A modest gain appears only once the bath becomes fast enough to place weight near ω_0 (up to 1.24 at $\gamma = \omega_0$, for $\lambda_{\mathrm{DL}} = 0.1$); for $\gamma = 5\,\omega_0$ the dynamics is Markovian to within 3% ($T = 0.5\,\omega_0$; the hierarchy is unstable at $T = 0.1\,\omega_0$, Appendix A). Ohmic baths, which are broad and featureless, give gains of at most 9% (1.01–1.09). These trends are consistent with the following picture. A slow bath acts on the battery as a quasi-static random transverse field, whose variance grows with λ_{DL} and T. This field tilts the quantization axis and dephases the energy-basis coherences on top of the golden-rule decay—an effect that a Markovian treatment, which samples J only at ω_0, cannot see. Memory without spectral weight at ω_0 is therefore a liability, not a resource.

A controlled test separates the two. Detuning the peak of an underdamped bath to $\omega_r = 0.6$–$1.4\,\omega_0$ at fixed width keeps the memory time, and a non-Markovianity of the same order as on resonance, but removes the weight at ω_0 [Fig. 3(b),(c)]. The gain then disappears. For $\lambda_{rc} = 0.05$ and $\kappa = 0.01\,\omega_0$ ($\tau_B\omega_0 = 100$), $\mathcal{N}_{\mathrm{BLP}}$ falls only from 4.4 to 1.0–2.3, whereas the gain falls from 82 to 0.85–0.95, i.e. below the Markovian value. Conversely, a resonant bath with $r = 1$ gives a gain of 1.54 and a Drude–Lorentz bath with $\gamma = \omega_0$ a gain of 1.24, although their backflow is negligible for every pair we sampled: over 17 pairs of orthogonal pure states (the class that

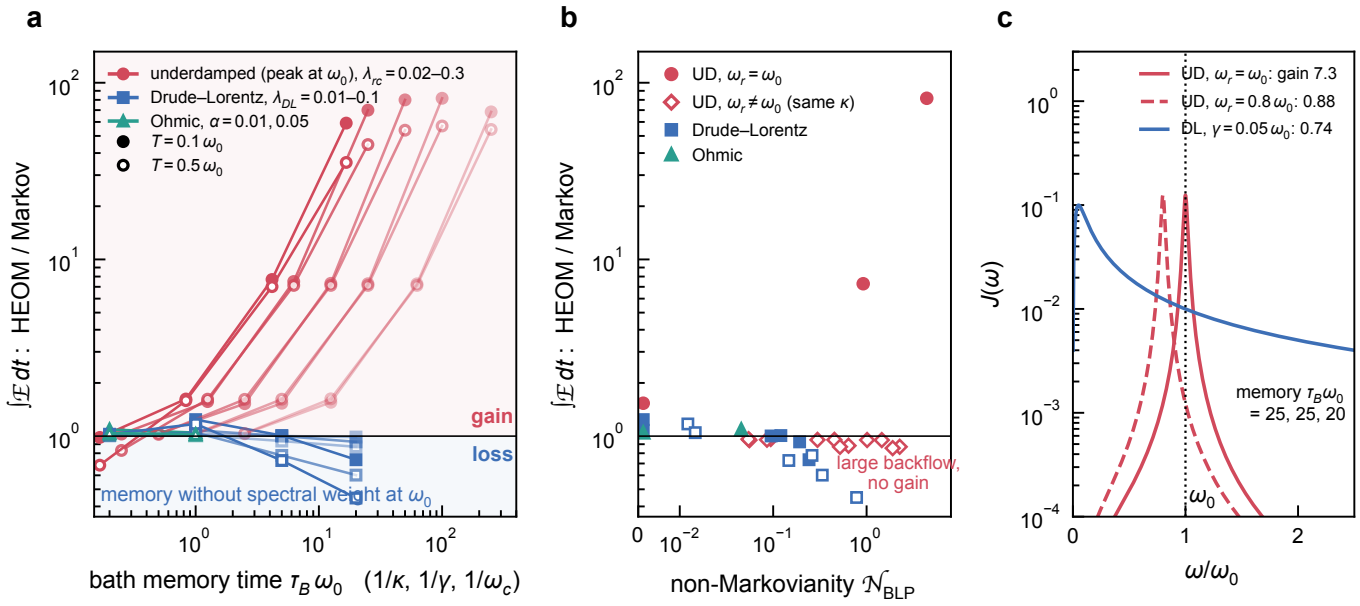


FIG. 3. **The non-Markovian gain requires spectral weight at the battery frequency, not long memory.** (a) Time-integrated stored ergotropy from HEOM relative to the golden-rule Markovian limit with the same $J(\omega_0)$, versus the bath memory time τ_B ($1/\kappa$, $1/\gamma$ or $1/\omega_c$), for underdamped (peaked at ω_0), Drude–Lorentz and Ohmic spectral densities. Filled symbols: $T = 0.1\,\omega_0$; open symbols: $T = 0.5\,\omega_0$; darker colours: stronger coupling. Slow overdamped baths reduce the stored work to as little as 0.45 of the Markovian value, whereas resonant peaked baths enhance it by up to a factor of 82. (b) The same ratio versus the non-Markovianity $\mathcal{N}_{\rm BLP}$ for resonant and detuned ($\omega_r = 0.6$–$1.4\,\omega_0$, same κ) underdamped baths ($\lambda_{rc} = 0.05$, $T = 0.1\,\omega_0$), Drude–Lorentz baths ($\lambda_{\rm DL} = 0.03, 0.1$; filled $T = 0.1$, open $T = 0.5\,\omega_0$) and Ohmic baths; $\mathcal{N}_{\rm BLP}$ is the larger of the values for $(|e\rangle, |g\rangle)$ and $(|+\rangle, |-\rangle)$; points with $\mathcal{N}_{\rm BLP} = 0$ are drawn at the left edge. (c) Spectral densities with comparable memory but opposite outcomes; the legend gives the gain.

contains the optimal pair for a qubit [58]), the largest value is 2×10^{-4}, four orders of magnitude below the detuned baths. Across all baths, $\mathcal{N}_{\rm BLP}$ does not predict the gain [Fig. 3(b)]: the slow Drude–Lorentz bath at $T = 0.5\,\omega_0$ has $\mathcal{N}_{\rm BLP} = 0.78$ and stores the least work (0.45 of the Markovian value). Information backflow thus does not predict the gain: it is not sufficient, and a sizable gain occurs with backflow that is negligible for all sampled state pairs.

The same baths expose a further failure of second-order treatments. With a tilted coupling and a slow Drude–Lorentz bath the Bloch–Redfield equation produces density matrices with negative eigenvalues (down to -0.15 for $\lambda_{\rm DL} = 0.1$, $\gamma = 0.05$, $T = 0.5$), together with a time-integrated ergotropy twenty times larger than the exact value (123 versus 6.0). It therefore cannot be used to decide whether a slow bath helps or hurts.

Figure 3(c) summarizes the conclusion. What the battery needs from its environment is spectral weight at ω_0 in a narrow band, which turns dissipation into coherent exchange with a bath mode; long memory is a by-product of a narrow band, not the cause of the gain. This agrees with the recent suggestion that memory itself is not required [55], but here it is established with exact dynamics and with a counterexample in which memory is long and the effect is negative. It also identifies the quantity that a battery designer should engineer: the spectral density at the battery frequency, rather than a measure of non-Markovianity such as information backflow [57].

V. THE DECOUPLING TOLL

The ergotropy (7) is the work extractable from the battery *after* it has been disconnected from the bath. Disconnection, however, costs work: removing the interaction term changes the energy of the global state by $W_{\rm off} = -\langle H_I \rangle$ [Eq. (8)]. For batteries charged by thermalization, this connection and disconnection work has been computed numerically and shown to limit the efficiency of a charging cycle [36, 37, 59]. For a general bipartite system, the ergotropy left after a sudden switch-off minus its quench cost, the switch-off ergotropy, has been defined and compared with the local ergotropy extractable without decoupling [33, 35]. Here we derive the cost in closed form for a qubit battery coupled to a bosonic bath, track it along the non-Markovian dynamics, and minimize it in finite time (Sec. VI).

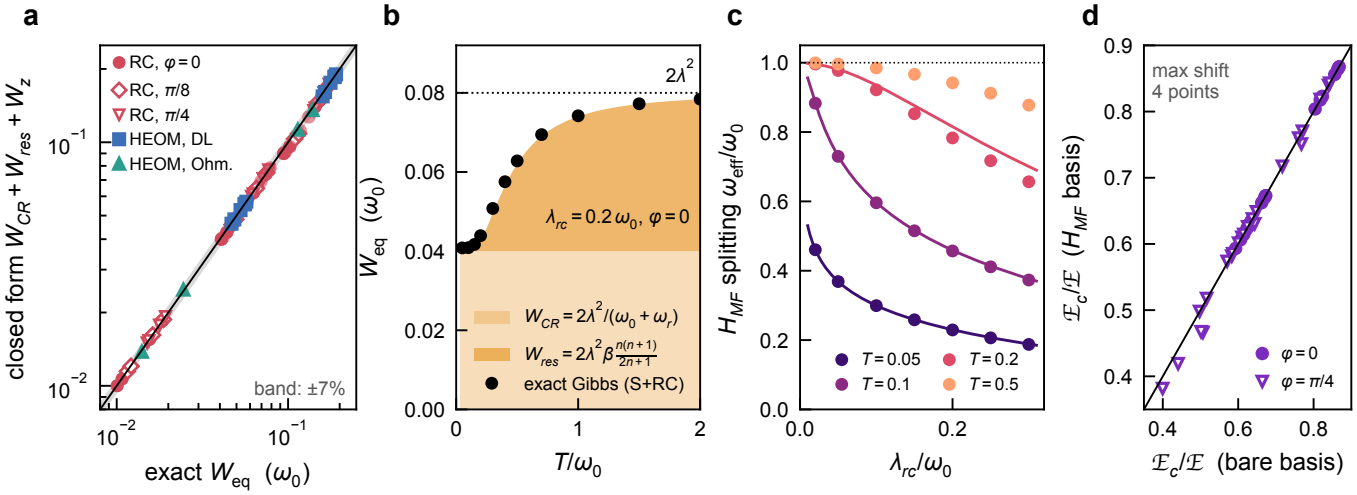


FIG. 4. **The decoupling toll has a closed form, whereas mean-force ergotropy collapses at low temperature.** (a) Closed-form toll $\cos^2\varphi\,[W_{\rm CR}+W_{\rm res}(T)]+\sin^2\varphi\,W_z$ [Eqs. (10)–(12)] versus exact values from the system–reaction-coordinate Gibbs state ($\varphi=0$: $T=0.05$–$2\,\omega_0$; $\varphi=\pi/8,\pi/4$: $T=0.1$–$1\,\omega_0$), HEOM steady states for Drude–Lorentz baths and long-time HEOM values for Ohmic baths. Grey band: ±7%. (b) Counter-rotating binding $W_{\rm CR}$ and resonant thermal contribution $W_{\rm res}$ for $\lambda_{rc}=0.2\,\omega_0$, compared with exact values. (c) Level splitting of the Hamiltonian of mean force; lines: low-temperature form (14). Because $\mathcal{E}_{\rm MF}=(\omega_{\rm eff}/\omega_0)\mathcal{E}$ for parity-symmetric coupling, mean-force ergotropy vanishes as $T\to 0$ irrespective of the state. (d) Coherent fraction of the ergotropy in the mean-force versus the bare eigenbasis: identical for $\varphi=0$, within four percentage points for $\varphi=\pi/4$.

A. Second-order dynamics of the interaction energy

Starting from the product state at $t=0$, second-order perturbation theory in H_I gives $\langle H_I\rangle(t)=2\int_0^t d\tau\,\mathrm{Im}[G(\tau)C(\tau)]$, where $G(\tau)=\langle Q(\tau)Q(0)\rangle$ is the free system correlation function. For $Q=\sigma_x$ it reads $G(\tau)=p_e e^{i\omega_0\tau}+p_g e^{-i\omega_0\tau}$, because coherences do not enter at this order. Inserting Eq. (2) yields

$$\langle H_I\rangle(t)=\frac{2}{\pi}\int_0^\infty d\omega\,J(\omega)\Big\{\big[\bar n p_e-(\bar n+1)p_g\big]\times\frac{1-\cos(\omega+\omega_0)t}{\omega+\omega_0}+\big[(\bar n+1)p_e-\bar n p_g\big]\times\frac{1-\cos(\omega-\omega_0)t}{\omega_0-\omega}\Big\},\tag{9}$$

with $\bar n=\bar n(\omega)$. The first term stems from the counter-rotating part of the coupling. It describes the dressing of the battery by virtual bath excitations, which builds up on the time scale $1/(\omega+\omega_0)$ while oscillating at the frequency $\omega+\omega_0$. The second term stems from resonant exchange.

B. Closed form of the equilibrium toll

At long times and with Gibbs populations, $p_e/p_g=e^{-\beta\omega_0}$, the numerator $(\bar n+1)p_e-\bar n p_g$ of the resonant term vanishes exactly at $\omega=\omega_0$ (detailed balance), so the principal value is regular. The equilibrium toll then takes the closed form

$$W_{\rm eq}=W_{\rm CR}+W_{\rm res}(T),\tag{10}$$
$$W_{\rm CR}=\frac{2}{\pi}\int d\omega\,J(\omega)\,\frac{(\bar n+1)p_g-\bar n p_e}{\omega+\omega_0},$$
$$W_{\rm res}=\frac{2}{\pi}\,\mathrm{P}\!\int d\omega\,J(\omega)\,\frac{\bar n p_g-(\bar n+1)p_e}{\omega_0-\omega}.$$

For a resonant reaction coordinate ($\omega_r=\omega_0$) in the narrow-peak limit $\kappa\ll\omega_0$ both terms are elementary:

$$W_{\rm eq}(T)=\frac{2\lambda_{rc}^2}{\omega_0+\omega_r}+2\lambda_{rc}^2\beta\,\frac{\bar n(\bar n+1)}{2\bar n+1},\tag{11}$$

with $\bar n=\bar n(\omega_0)$. For a finite width, Eq. (10) must be integrated with $J_{\rm UD}$; at $\lambda_{rc}=0.3$ this lowers $W_{\rm CR}$ by 7% for $r=0.2$ and by a factor of 2.5 for $r=5$, where the peak is broader than ω_0. At zero temperature $W_{\rm eq}=2\lambda_{rc}^2/(\omega_0+\omega_r)$ is twice the Bloch–Siegert binding energy $E_b=\lambda_{rc}^2/(\omega_0+\omega_r)$ of the dressed ground state, as required by the Hellmann–Feynman relation $\langle H_I\rangle=2E^{(2)}$ for the second-order energy shift $E^{(2)}=-E_b$. The resonant term $W_{\rm res}$ vanishes at $T=0$. At finite temperature it arises because thermally occupied Jaynes–Cummings doublets, split by $\pm\lambda_{rc}\sqrt{m+1}$ in the sector with m thermal quanta, preferentially populate their lower member; at high temperature it saturates at λ_{rc}^2, so that $W_{\rm eq}\to 2\lambda_{rc}^2$ [Fig. 4(b)].

For the tilted coupling $Q=\cos\varphi\,\sigma_x+\sin\varphi\,\sigma_z$ the static component contributes $\sin^2\varphi\,\langle\sigma_z^2\rangle=\sin^2\varphi$ to $G(\tau)$, which adds a polaron binding term:

$$W_{\rm eq}(\varphi)=\cos^2\varphi\,\big[W_{\rm CR}+W_{\rm res}(T)\big]+\sin^2\varphi\,W_z,\tag{12}$$

with $W_z = (2/\pi)\int d\omega\, J(\omega)/\omega$, i.e., $W_z = 2\lambda_{rc}^2/\omega_r$ for the reaction coordinate. This term is independent of temperature at second order.

Equations (10)–(12) agree with all exact results [Fig. 4(a)].

- For the reaction coordinate (36 Gibbs states, $\varphi = 0, \pi/8, \pi/4$, $T = 0.1$–1) the deviation from the exact Gibbs state is below 0.7% for $\lambda_{rc} \le 0.1$ and at most 6.1% at $\lambda_{rc} = 0.3$, as expected from fourth-order corrections.
- For Drude–Lorentz baths the deviation from HEOM steady states is 0.1–3.0% (at most 0.7% for $\gamma = 5\,\omega_0$).
- For Ohmic baths it is at most 2.2% relative to the long-time HEOM value.

The toll is therefore set by the spectral density and the temperature alone, through the same formula for structured and featureless baths. It scales as λ^2, i.e., with the same coupling that produces the non-Markovian gain.

C. Limits of mean-force ergotropy as withdrawable work

A natural alternative to paying the toll is to define the battery energy at strong coupling through the Hamiltonian of mean force [38, 39],

$$H_{\rm MF} = -T \ln \frac{{\rm Tr}_E\, e^{-\beta H}}{Z_E}, \tag{13}$$

which makes the reduced equilibrium state a Gibbs state, and to quantify stored work as the ergotropy $\mathcal{E}_{\rm MF}$ with respect to $H_{\rm MF}$. For parity-symmetric coupling, $Q = \sigma_x$, the global parity $\sigma_z e^{i\pi \sum_k b_k^\dagger b_k}$ is conserved. Hence $H_{\rm MF} = \frac{\omega_{\rm eff}}{2}\sigma_z$ up to a constant. Since the ergotropy of a qubit is linear in its level splitting, $\mathcal{E}_{\rm MF} = (\omega_{\rm eff}/\omega_0)\,\mathcal{E}$ holds exactly, and so does the split into coherent and incoherent parts. The effective splitting is fixed by the excited-state population p of the mean-force Gibbs state, $\omega_{\rm eff} = T\ln[(1-p)/p]$. At low temperature p is dominated by the virtual excitations of the dressed ground state rather than by the Boltzmann factor, which gives

$$\omega_{\rm eff} \simeq T \ln \frac{1-p}{p}, \qquad p \simeq \frac{\lambda_{rc}^2}{(\omega_0+\omega_r)^2} + e^{-\omega_0/T}. \tag{14}$$

Once $T \lesssim \omega_0/\ln[(\omega_0+\omega_r)^2/\lambda_{rc}^2]$, therefore, $\omega_{\rm eff}$ decreases linearly with T and vanishes as $T \to 0$. Even weak coupling is affected: at $T = 0.1\,\omega_0$, $\omega_{\rm eff}/\omega_0 = 0.73$ for $\lambda_{rc} = 0.05$ and 0.37 for $\lambda_{rc} = 0.3$, and at $T = 0.05\,\omega_0$ it reaches 0.19 for $\lambda_{rc} = 0.3$ [Fig. 4(c)]. Equation (14) reproduces these values to within 1% at $T \le 0.1\,\omega_0$. Mean-force ergotropy thus collapses at low temperature for every state. This is precisely the regime of superconducting batteries, so it cannot serve as a measure of stored work there. It is in line with the recent observation that the reduced equilibrium state does not determine a local Hamiltonian and temperature unambiguously [42, 43]. Conversely, the mean-force Gibbs state can carry coherent ergotropy with respect to the bare Hamiltonian at strong coupling [40]; withdrawing it requires disconnecting the battery and therefore paying the toll (10). For the shared bath, the exactly dark singlet (Sec. III) makes the dynamics non-ergodic, so the mean-force Gibbs state is never reached from these initial states and $H_{\rm MF}$ does not describe the stationary battery.

The choice of energy operator also leaves the split into coherent and incoherent ergotropy essentially unchanged [Fig. 4(d)]. The split is identical for $\varphi = 0$ and shifts by at most four percentage points for $\varphi = \pi/4$, where $H_{\rm MF}$ acquires small off-diagonal elements. In contrast, the coupling geometry itself, i.e., changing φ from 0 to $\pi/4$ at fixed λ_{rc}, changes the coherent fraction by up to 19 points, because the σ_z component dephases the battery. The operationally meaningful quantity at strong coupling is therefore not $\mathcal{E}_{\rm MF}$ but the work that can actually be withdrawn: the net work $\mathcal{E} - W_{\rm off}$ if the battery is disconnected, or the local ergotropy if it is not. Section VI determines when the net work is positive, how to maximize it, and how it compares with extraction in place.

VI. HARVESTING CRITERION AND OPTIMAL DECOUPLING

Figure 1(b) shows that the toll of Sec. V is of the same order as the revivals that make up the non-Markovian gain. Whether a revival is a resource therefore depends on how the battery is disconnected. In this section we derive the net work for the two limiting decoupling protocols, obtain the criterion that decides when a revival can be harvested, and construct the finite-time ramp that reaches the optimal limit. We treat the storage protocol with $\varphi = 0$ and the resonant reaction coordinate first, extend the result to finite temperature and tilted coupling, and finally compare decoupling with extraction in place.

A. Revivals and the dressing they carry

At $T = 0$ the rotating-wave solution is exact in the single-excitation sector and, as shown in Sec. III, accurate for storage up to $\lambda_{rc} = 0.3\,\omega_0$. The excited-state amplitude is $c\,u(t)$ with $c = \cos\frac{\theta}{2}$, $s = \sin\frac{\theta}{2}$, and

$$u(t) = e^{-\kappa t/4}\Big[\cos\Omega t + \frac{\kappa}{4\Omega}\sin\Omega t\Big], \qquad \Omega = \sqrt{\lambda_{rc}^2 - \kappa^2/16}. \tag{15}$$

Because $\dot u \propto \sin\Omega t$, the revivals peak exactly at $t_n = n\pi/\Omega$, where their depth is

$$x_n \equiv |u(t_n)|^2 = \exp\Big(-\frac{n\pi\kappa}{2\Omega}\Big) \simeq e^{-2\pi n r}. \tag{16}$$

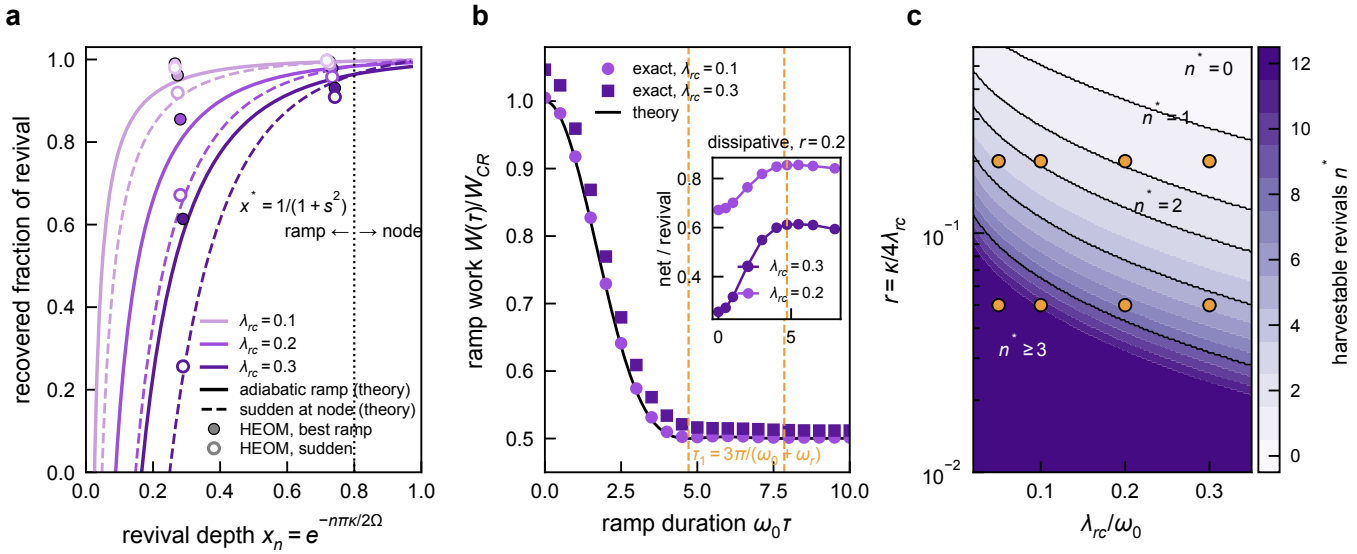


FIG. 5. **In second-order theory a revival yields net work after disconnection only if it exceeds the system–bath binding energy (half the sudden-decoupling toll), a bound that a $\cos^2$ ramp lasting a few battery periods nearly reaches.** (a) Recovered fraction of the first revival versus the revival depth x_n. Lines: Eq. (19) for adiabatic (solid) and sudden-at-node (dashed) decoupling; the optimal protocol switches at $x^* = 1/(1+s^2)$. Symbols: best finite-time ramp (filled) and best sudden decoupling (open) from HEOM with a time-dependent coupling, $T = 0.1\,\omega_0$. (b) Work to remove an equilibrated dressing with a $\cos^2$ ramp of duration τ. Line: Eq. (22); symbols: exact closed dynamics. In second-order theory for a single bath mode the diabatic excess vanishes at $\tau_k = (2k+1)\pi/(\omega_0+\omega_r)$ (dashed). Inset: net recovered fraction with dissipation, which plateaus between τ_1 and $\approx 6.5/\omega_0$. (c) Number of net-harvestable revivals n^* predicted by Eq. (19) at $T \to 0$. Symbols: parameters at which HEOM yields positive net work from the first revival ($T = 0.1\,\omega_0$).

Inserting $\langle\sigma_z\rangle = 2c^2x_n - 1$ and $|\langle\sigma_+\rangle| = cs\sqrt{x_n}$ into the qubit ergotropy gives the revival ergotropy

$$\mathcal{E}_n = \frac{\omega_0}{2}\left[2c^2x_n - 1 + \sqrt{(2c^2x_n-1)^2 + 4c^2s^2x_n}\right] \simeq \frac{\omega_0 \sin^2\theta}{4}\,x_n \qquad (x_n \ll 1), \tag{17}$$

which agrees with the HEOM revival at $T = 0.1\,\omega_0$ to within 3% for $\lambda_{rc} \leq 0.2$ and 7% at $\lambda_{rc} = 0.3$ (where it underestimates).

The toll at t_n follows from the counter-rotating term of Eq. (9). For the reaction coordinate it consists of two parts:

$$W_{\rm off}^{\rm CR}(t) \simeq W_{\rm CR}\left[p_g(t) - p_g(0)\,e^{-\kappa t/2}\cos(\omega_0+\omega_r)t\right]. \tag{18}$$

The first part is the equilibrated dressing. It follows the instantaneous ground-state weight $p_g(t)$ on the fast time scale $1/(\omega_0+\omega_r)$, because only the ground-state component is bound at $T = 0$. The second part is the memory of the quench at $t = 0$. It oscillates at $\omega_0 + \omega_r$, carries the initial weight $p_g(0) = s^2$, and decays at the rate $\kappa/2$ of the reaction coordinate—the same rate that sets the revival depth. At t_n its envelope is therefore x_n again. Equation (18) reproduces the HEOM toll $W_{\rm off}(t)$ over the first three revival periods with a root-mean-square error of 0.004–$0.006\,\omega_0$ at $\lambda_{rc} = 0.2$ and 0.008–$0.015\,\omega_0$ at $\lambda_{rc} = 0.3$ ($T = 0.1\,\omega_0$).

B. Two decoupling limits and the harvesting criterion

Two limiting protocols bracket the work needed to disconnect the battery at a revival. (i) *Sudden decoupling at a node.* Switching the coupling off instantaneously at a time where $\cos(\omega_0+\omega_r)t = 1$ costs $W_{\rm CR}[p_g(t_n) - p_g(0)x_n]$. The nodes are spaced by $2\pi/(\omega_0+\omega_r)$, finer than the revival width $\sim \pi/2\lambda_{rc}$ for $\lambda_{rc} \lesssim 0.2\,\omega_0$ and comparable to it at $\lambda_{rc} = 0.3\,\omega_0$, so a node is always close to the revival peak. (ii) *Adiabatic decoupling.* Ramping the coupling down slowly compared with $1/(\omega_0+\omega_r)$ lets the dressing follow the coupling and returns half of its energy, so that the cost is the binding energy $E_b = W_{\rm CR}/2$ per unit ground-state weight, whether or not the quench oscillation is still present. The total, $W_{\rm CR}\,p_g(t_n)/2$, contains no quench-memory term; it depends on x_n only through $p_g(t_n)$. At finite temperature both protocols pay in addition the part of the resonant toll that has built up, $W_{\rm res}(T)(1-x_n)$. The work that can be withdrawn from the n-th revival is therefore

$$\mathcal{E}_n^{\rm net} \simeq \mathcal{E}_n - W_{\rm CR}\,\min\left[p_g(t_n) - p_g(0)x_n,\ \tfrac{1}{2}p_g(t_n)\right] - W_{\rm res}(T)\,(1-x_n). \tag{19}$$

This is the harvesting criterion: a revival is a resource only if $\mathcal{E}_n^{\rm net} > 0$. Equation (19) gives a precise meaning to the intuition that the revival must exceed the toll.

What must be exceeded is not $W_{\rm eq}$ but, for the optimal protocol, the binding energy $p_g W_{\rm CR}/2$, i.e., half the sudden toll, plus the resonant thermal term.

At $T=0$, where $p_g(t_n)=1-c^2x_n$ and $p_g(0)=s^2$, the cost of sudden decoupling at a node reduces to $W_{\rm CR}(1-x_n)$. It is lower than the adiabatic cost only for deep revivals,

$$x_n > x^* = \frac{1}{1+s^2}, \tag{20}$$

i.e., $x^*=0.8$ for $\theta=\pi/3$, which requires $r<\ln(1.25)/2\pi\approx 0.036$ for the first revival. A larger initial ground-state weight widens the window for sudden decoupling. All of our parameter points have $x_1\le 0.73$, so Eq. (19) predicts that the adiabatic limit is optimal throughout, and the exact dynamics agrees: of the 16 points with $\varphi=0$, the best finite ramp outperforms sudden decoupling at 15 and matches it to within 0.1% at the remaining one ($\lambda_{rc}=0.05$, $r=0.05$, $T=0.5\,\omega_0$). For shallow revivals, $x_n\ll 1$, Eqs. (17) and (19) with the optimal protocol give the index of the last harvestable revival,

$$n^* \simeq \frac{1}{2\pi r}\ln\frac{\omega_0(\omega_0+\omega_r)\sin^2\theta}{4\lambda_{rc}^2}. \tag{21}$$

Stronger coupling increases the number of revivals per unit time, but it reduces the number that can be harvested, because the binding energy grows as λ_{rc}^2 while the revival ergotropy does not. For $\lambda_{rc}=0.1$ and $r=0.05$, about eleven revivals can be harvested; for $\lambda_{rc}=0.3$ and $r=0.2$, only the first [Fig. 5(c)].

We tested Eq. (19) against exact HEOM with a time-dependent coupling (Sec. II), for $\lambda_{rc}\in\{0.05,0.1,0.2,0.3\}$, $r\in\{0.05,0.2\}$ and $T\in\{0.1,0.5\}\,\omega_0$, optimizing the start time and duration of a $\cos^2$ ramp [Fig. 5(a)]. At $T=0.1\,\omega_0$ the predicted net work deviates from the exact value by at most $0.009\,\omega_0$, and it underestimates the net work wherever the deviation exceeds $0.002\,\omega_0$ except at $\lambda_{rc}=0.3$, $r=0.05$. The recovered fraction of the first revival is at least 96% for $\lambda_{rc}\le 0.1$, but it drops to 86% at $\lambda_{rc}=0.2$ and to 61% at $\lambda_{rc}=0.3$ for $r=0.2$. Sudden decoupling recovers only 26% of the revival at $\lambda_{rc}=0.3$, $r=0.2$.

C. Finite-time decoupling ramp

The adiabatic limit seems to require a slow ramp, during which the revival decays. A second-order calculation for a ramp $f(t/\tau)$ from 1 to 0 acting on an equilibrated dressing shows that it does not. The work is

$$W(\tau)=\frac{W_{\rm CR}}{2}\Big[1+|F(\nu)|^2\Big], \qquad F(\nu)=\int_0^1 ds\,\dot f(s)\,e^{i\nu s}, \tag{22}$$

with $\nu=(\omega_0+\omega_r)\tau$. It interpolates between the sudden toll $W_{\rm CR}$ at $\tau\to 0$ and the binding energy $W_{\rm CR}/2$ at $\tau\to\infty$. For the $\cos^2$ ramp, $f(s)=\cos^2(\pi s/2)$, the diabatic excess is $|F(\nu)|^2=\pi^4\cos^2(\nu/2)/(\pi^2-\nu^2)^2$. Besides decaying as ν^{-4}, it vanishes at $\nu=(2k+1)\pi$ with $k\ge 1$, so that in this single-mode, second-order theory the adiabatic limit is reached at the finite ramp durations

$$\tau_k=\frac{(2k+1)\pi}{\omega_0+\omega_r}, \qquad \tau_1=\frac{3\pi}{\omega_0+\omega_r}\approx\frac{4.71}{\omega_0}. \tag{23}$$

Equation (22) agrees with the exact closed system–reaction-coordinate dynamics to within 0.7% for $\lambda_{rc}=0.1$ and 7% for $\lambda_{rc}=0.3$, the latter set by fourth-order corrections [Fig. 5(b)]. At τ_1 the exact work is $0.502\,W_{\rm CR}$ for $\lambda_{rc}=0.1$.

The zeros are a property of a single bath mode in second-order theory. For a continuous spectral density the second-order excess, $(1/\pi)\int d\omega\,J(\omega)|F((\omega+\omega_0)\tau)|^2/(\omega+\omega_0)$ at $T=0$, samples $|F|^2$ over the whole band and no longer vanishes. At τ_1 it amounts to 0.2%, 0.8%, 3.2% and 8.9% of E_b for underdamped baths with $r=0.05$, 0.2, 1 and 5 ($\lambda_{rc}=0.3$), and to 1.7% for a Drude–Lorentz bath with $\gamma=\omega_0$. Because $|F|^2$ decays as ν^{-4}, it falls below 0.2% of E_b in all cases once $\omega_0\tau\approx 8$. The robust design rule is therefore that a $\cos^2$ ramp lasting a few battery periods, $\tau\gtrsim\tau_1$, reaches the adiabatic limit to within the bath width; τ_1 is its shortest duration for a narrow resonant bath.

With dissipation, the ramp must also be short compared with the revival lifetime. The net work then plateaus from τ_1 to $\omega_0\tau\approx 6.5$ [Fig. 5(b), inset]. For $\lambda_{rc}=0.3$ and $r=0.2$ it is 0.0516–$0.0519\,\omega_0$ for $\omega_0\tau$ between 4.7 and 6.5, 2.4 times the value for sudden decoupling ($0.0217\,\omega_0$), and it is only 3% lower at $\omega_0\tau=8$. The rotating exchange with the reaction coordinate continues during the ramp, but this is compensated by starting the ramp earlier, so that the exchange angle accumulated under the reduced coupling brings the battery to its revival at the end of the ramp. The optimal protocol is therefore adiabatic with respect to the counter-rotating dressing and effectively sudden with respect to resonant exchange. It requires only control of the coupling strength over a few periods of the battery, which tunable couplers on superconducting platforms, where the extraction of coherent ergotropy has been demonstrated [8], provide.

D. Finite temperature and tilted coupling

At finite temperature the revival ergotropy itself decreases (Sec. III). Two processes contribute: thermal photons present in the reaction coordinate at $t=0$ randomize the phases of the vacuum Rabi oscillation, and photons absorbed from the residual bath during the revival degrade it further. In the rotating-wave reaction-coordinate dynamics they act multiplicatively, $\mathcal{E}_n(T)\simeq\mathcal{E}_n^{\rm init}\mathcal{E}_n^{\rm abs}/\mathcal{E}_n(0)$, to within about 3% for $T\le\omega_0$. This suggests a cumulant resummation in the thermal

occupation $\bar{n}$,

$$\mathcal{E}_n(T) \simeq \max_t \, \mathcal{E}_n(0;t)\, e^{\bar{n}\, c_1(t)}, \quad c_1 = \frac{\partial \ln \mathcal{E}_n}{\partial \bar{n}}\Big|_{\bar{n}=0}, \quad (24)$$

where the first-order coefficient $c_1(t)$ is computed exactly from a block-matrix exponential of the reaction-coordinate Liouvillian, and the maximization over time accounts for the thermal shift of the revival. Equation (24) reproduces the exact rotating-wave revival to within 6% for $r = 0.05$ and 15% for $r = 0.2$ up to $\bar{n} = 1$ ($T \approx 1.4\,\omega_0$), and the HEOM revival at $T = 0.5\,\omega_0$ to within 3% for $\lambda_{rc} \le 0.2$ and 8% at $\lambda_{rc} = 0.3$. Inserted into Eq. (19) with the thermal toll (11), it predicts the net work at $T = 0.5\,\omega_0$ to within $0.007\,\omega_0$, with the correct sign at every point. At $\lambda_{rc} = 0.3$, $r = 0.2$ none of the decoupling protocols we tested yields net work: the best ramp gives $-0.016\,\omega_0$, against a prediction of $-0.023\,\omega_0$. Temperature thus taxes a revival twice: it reduces $\mathcal{E}_n$ and adds $W_{\rm res}(T)$. At $T \gtrsim \omega_0$ the revival falls below 30% of its zero-temperature value, while the toll approaches $2\lambda_{rc}^2$, and net harvesting essentially ceases.

For tilted coupling, the static polaron term of Eq. (12) enters Eq. (19) as $\sin^2\varphi\, W_z/2$ for adiabatic and $\sin^2\varphi\, W_z(1-x_n)$ for sudden decoupling. The revival is reduced as well: exchange proceeds at the rate $\lambda_{rc}\cos\varphi$, and the σ_z component dephases the battery by the independent-boson factor $e^{-\Gamma(t_n)}$, with $\Gamma(t) = \frac{4}{\pi}\sin^2\varphi \int d\omega\, J(\omega) \coth\frac{\beta\omega}{2}\,(1-\cos\omega t)/\omega^2$ evaluated at the revival. Because $J_{\rm UD} \propto \omega$ at low frequency, $\Gamma(t)$ grows logarithmically at $T = 0$ and linearly at finite temperature, so it has no long-time limit; at the revival ($\lambda_{rc} = 0.2$, $r = 0.05$, $\varphi = \pi/4$) it exceeds the single-mode phase average $4\lambda_{rc}^2 \sin^2\varphi/\omega_r^2$ by factors of 1.8 ($T = 0.1\,\omega_0$) and 3.0 ($T = 0.5\,\omega_0$), so the finite-time value must be used. An exact polaron transformation shows that the leading correction beyond this picture is a two-phonon Franck–Condon exchange, $|e,0\rangle \leftrightarrow |g,2\rangle$; including it reproduces the exact revival to within 6% for $\lambda_{rc} \le 0.2$. With the revival taken from the dynamics, Eq. (19) including W_z predicts the HEOM net work for $\varphi = \pi/4$, $\lambda_{rc} = 0.2$ and $r = 0.05$ to within $0.014\,\omega_0$ at both temperatures; with the analytic independent-boson revival the error is $0.015\,\omega_0$ at $T = 0.1\,\omega_0$ but $0.04\,\omega_0$ at $T = 0.5\,\omega_0$, where thermal cross terms are missing. At $\lambda_{rc} = 0.3$ and $\varphi \neq 0$, however, a resonant cross term between the σ_x and σ_z couplings grows secularly during the dynamics and makes the transient toll non-perturbative. The equilibrium toll (12) remains accurate there, but the net work must be computed numerically.

E. Extraction without disconnection

The toll is paid only if the battery is disconnected. Work can also be withdrawn in place, by a unitary on the battery alone applied while the coupling stays on. The maximum work extracted in this way is the local ergotropy [33, 34]. For a qubit it has a closed form [33], which for the coupling $Q = \mathbf{q}\cdot\boldsymbol{\sigma}$ takes a particularly simple shape. A local unitary rotates the Bloch vector $\mathbf{r}$ and the correlation vector $c_a = \lambda_{rc}\langle\sigma_a \otimes (a + a^\dagger)\rangle$ by the same rotation $R \in \mathrm{SO}(3)$, so the energy after the unitary is $\mathrm{Tr}[A^{\rm T}R]$ with $A = \frac{\omega_0}{2}\hat{\mathbf{z}}\,\mathbf{r}^{\rm T} + \mathbf{q}\,\mathbf{c}^{\rm T}$. The minimum over SO(3) of this linear function is $-\|A\|_*$, the sum of the singular values of the rank-two matrix A, so that

$$\mathcal{E}_{\rm loc} = \mathrm{Tr}\, A + \|A\|_*, \quad (25)$$

which reduces to the qubit ergotropy for $\lambda_{rc} = 0$. Equation (25) is the case $\det A = 0$ of the general qubit formula of Ref. [33], for which the correction for a negative determinant vanishes.

We evaluated Eq. (25) along the HEOM dynamics, with the correlation vector $c_a = \sum_k \mathrm{Tr}[\sigma_a \rho^{(k)}]$ obtained from the first-tier auxiliary density operators, and maximized it over the revival window, as for the decoupling protocols. In-place extraction outperforms decoupling at every point we computed: it exceeds the best finite-time ramp at all 18 points ($\varphi = 0$ with $\lambda_{rc} = 0.05$–0.3, $r = 0.05, 0.2$ and $T = 0.1, 0.5\,\omega_0$, and $\varphi = \pi/4$ with $\lambda_{rc} = 0.2$, $r = 0.05$). The advantage is negligible at weak coupling and grows with the toll. At $\lambda_{rc} = 0.3$ and $r = 0.2$, in-place extraction yields $0.092\,\omega_0$ against $0.052\,\omega_0$ for the best tested ramp and $0.022\,\omega_0$ for switch-off at $T = 0.1\,\omega_0$. At $T = 0.5\,\omega_0$ it yields $0.042\,\omega_0$, where every decoupling protocol we tested loses work. A qualitatively similar ordering was found for Jaynes–Cummings eigenstates in Ref. [33], which also shows that no general ordering between local and switch-off ergotropy exists. At $\varphi = 0$, the local ergotropy agrees with the ergotropy of the coupled battery to within -2% to $+9\%$, because the unitary can also lower the interaction energy. The coupled-state ergotropy used in the literature is therefore a good estimate of the work that can be withdrawn in place, but not of the work that can be withdrawn after disconnection.

In-place extraction requires a pulse on the battery that is short compared with $1/\lambda_{rc}$, so that the coupling acts negligibly during it; the free precession under H_S can be absorbed in the pulse phase. In-place extraction must, however, take place at the revival itself, within a time of order $1/\kappa$, after which the revival has decayed. Disconnection, and with it the toll, is therefore unavoidable whenever the energy is needed later than the revival, or by a load that is not coupled to the same environment, for example when a charged cell is moved to another register or kept in storage.

F. Collective storage

Practical batteries consist of many cells that share an environment. Figure 6 extends the storage protocol to $N = 1$–3 cells, each prepared in $|\psi\rangle$ and coupled collectively through $Q = \sum_i \sigma_x^i$ to one resonant bath, computed with HEOM. Three effects appear.

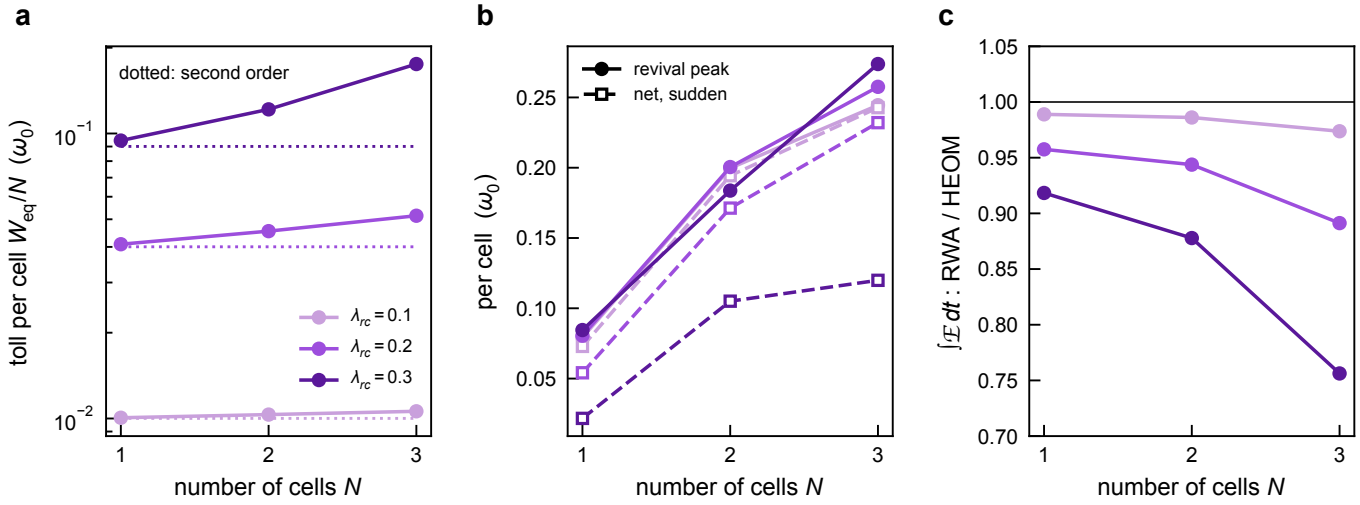


FIG. 6. **In collective storage the toll per cell exceeds its second-order value, while the collective revival grows faster at first.** N cells, each prepared in $|\psi\rangle$, share one resonant bath through $Q = \sum_i \sigma_x^i$ ($r = 0.2$, $T = 0.1\,\omega_0$). (a) Equilibrium toll per cell from the exact system–RC Gibbs state; dotted lines: second-order (extensive) value, Eq. (11). (b) Peak of the first revival (filled) and net work after sudden decoupling (open), per cell, from HEOM. (c) Ratio of rotating-wave to HEOM stored ergotropy.

First, the toll per cell is extensive only at second order. The exact equilibrium toll per cell rises with N above the second-order value of Eq. (11): for $N = 3$ it exceeds that value by 6% at $\lambda_{rc} = 0.1$, by 29% at 0.2 and by a factor of 1.9 at 0.3. Higher-order processes in which the bath mode mediates exchange between cells add binding energy, so the closed form applies per cell only while the collective coupling $\sqrt{N}\lambda_{rc}$ stays below about $0.2\,\omega_0$.

Second, the collective revival grows faster than the toll at first. Per cell, the revival peak rises from $0.08\,\omega_0$ for $N = 1$ to 0.18–$0.20\,\omega_0$ for $N = 2$ and 0.24–$0.27\,\omega_0$ for $N = 3$, because the cells exchange energy with the bath mode collectively. At $\lambda_{rc} = 0.3$ the fraction recovered by sudden decoupling rises from 26% ($N = 1$) to 57% ($N = 2$), before the superextensive toll reduces it to 44% at $N = 3$.

Third, the rotating-wave error grows with N: at $\lambda_{rc} = 0.3$ the rotating-wave solution underestimates the stored ergotropy by 8%, 12% and 24% for $N = 1$, 2 and 3. Collective strong coupling therefore requires a numerically exact treatment even for storage. For the narrowest bath, $r = 0.05$, the hierarchy is numerically unstable for $N = 2$ at $\lambda_{rc} = 0.3$ and for $N = 3$ at $\lambda_{rc} \geq 0.2$ (Appendix A).

Equations (19)–(25) complete the operational picture. A non-Markovian revival is a resource for a battery used in place without any threshold. For a battery that must be disconnected, it is a resource only when its depth x_n exceeds a threshold fixed by the binding energy, and a $\cos^2$ ramp lasting a few battery periods reaches that threshold at no cost in control complexity.

TABLE I. Parameters of Secs. III–VI in physical units for a qubit battery at $\omega_0/2\pi = 5$ GHz coupled to a resonant reaction-coordinate resonator ($\omega_r = \omega_0$). Revival period π/Ω with $\Omega = \lambda_{rc}\sqrt{1-r^2}$, revival lifetime $1/\kappa$ with $\kappa = 4r\lambda_{rc}$, in-place pulse bound $1/\lambda_{rc}$, and probability $P_{\rm pair} = [\lambda_{rc}/(\omega_0 + \omega_r)]^2$ of a correlated qubit–photon excitation left by sudden decoupling from the dressed ground state, Eq. (26). Temperatures $T = 0.1$ and $0.5\,\omega_0$ correspond to 24 and 120 mK.

λ_{rc}/ω_0	0.05	0.1	0.2	0.3
$\lambda_{rc}/2\pi$ (GHz)	0.25	0.5	1.0	1.5
$\kappa/2\pi$ (MHz), $r = 0.05$	50	100	200	300
$\kappa/2\pi$ (MHz), $r = 0.2$	200	400	800	1200
π/Ω (ns), $r = 0.05$	2.0	1.0	0.50	0.33
$1/\kappa$ (ns), $r = 0.05$	3.2	1.6	0.80	0.53
$1/\kappa$ (ns), $r = 0.2$	0.80	0.40	0.20	0.13
$1/\lambda_{rc}$ (ns)	0.64	0.32	0.16	0.11
$10^3\,P_{\rm pair}$, sudden	0.63	2.5	10	23

VII. EXPERIMENTAL FEASIBILITY

The model of Sec. II is the native Hamiltonian of a superconducting qubit coupled to a lossy resonator. The qubit is the battery, the resonator is the reaction coordinate, and the transmission line into which the resonator leaks is the Ohmic residual bath, so the qubit experiences exactly the underdamped spectral density $J_{\rm UD}$ of Eq. (3) with λ_{rc} set by the qubit–resonator coupling and κ by the resonator–line coupling. Capacitive coupling of a transmon [60] gives the transverse coupling $Q = \sigma_x$. A flux qubit coupled galvanically through its persistent

current realizes the tilted coupling: biased at a distance ε from its symmetry point, its persistent-current operator reads $\cos\varphi\,\sigma_x + \sin\varphi\,\sigma_z$ in the energy eigenbasis, with $\sin\varphi = \varepsilon/\omega_0$. A second qubit, coupled directly to the battery or through the same resonator, provides the charger of the two charging protocols. Intrinsic qubit relaxation, with times of tens of microseconds and longer, is slower than every time scale below by more than three orders of magnitude and can be neglected.

Table I expresses the parameter grid in physical units for $\omega_0/2\pi = 5$ GHz. A dilution refrigerator at 20 mK places such a qubit at $T = 0.083\,\omega_0$, so the lowest temperature studied, $T = 0.1\,\omega_0$ (24 mK), is the relevant one, and the thermal corrections of Secs. III and VI are small. The weakest couplings, $\lambda_{rc} \le 0.05\,\omega_0$, lie at the upper end of capacitive transmon–resonator coupling; $\lambda_{rc} = 0.1$–$0.3\,\omega_0$ is the ultrastrong-coupling regime, which has been reached and exceeded with galvanically coupled flux qubits [61–64]. The narrow baths $r = 0.05$–0.2 require a resonator linewidth of 50–1200 MHz, i.e. a strongly overcoupled resonator with a quality factor between about 100 and 4. All time scales of the revival dynamics are therefore between 0.1 and a few nanoseconds.

Decoupling ramp. The $\cos^2$ ramp of Sec. VI must last at least $\tau_1 = 3\pi/(2\omega_0) = 0.15$ ns, and it reaches the adiabatic limit to within 0.2% of the binding energy for any bath once $\omega_0\tau \approx 8$, i.e. 0.25 ns. It must also be short compared with the revival lifetime $1/\kappa$. At $\lambda_{rc} = 0.3\,\omega_0$, $r = 0.2$, where the net work plateaus for $\omega_0\tau = 4.7$–6.5 [Fig. 5(b), inset], this is a window of 0.15–0.21 ns and requires subnanosecond flux control of a tunable coupler [65]. At $\lambda_{rc} \le 0.1\,\omega_0$ and $r = 0.05$ the revival lives 1.6–3.2 ns (8 ns at $\lambda_{rc} = 0.02\,\omega_0$), and long ramps cost little. We computed the net work with HEOM for $\cos^2$ ramps up to $\omega_0\tau = 10\pi$, i.e. 1 ns at 5 GHz, again optimizing the start time. At $T = 0.1\,\omega_0$ a 1-ns ramp recovers 99.9%, 99.4% and 96.0% of the first revival for $\lambda_{rc} = 0.02$, 0.05 and $0.1\,\omega_0$, against 99.98%, 99.9% and 99.5% for a ramp of duration τ_1; at $T = 0.5\,\omega_0$ the 1-ns values are 99.9%, 98.7% and 93.9%. This loss is an order of magnitude smaller than the decay of the revival envelope during the ramp, $\kappa\tau/2 = 31\%$ at $\lambda_{rc} = 0.1\,\omega_0$, because the optimal ramp starts about $\tau/2$ before the revival and is centred on it. In this regime the toll is itself small—sudden decoupling already recovers at least 99.0% at $T = 0.1\,\omega_0$—so nanosecond flux pulses suffice. Lowering ω_0 lengthens all durations in proportion but raises T/ω_0: at $\omega_0/2\pi = 2$ GHz and 20 mK, $T = 0.21\,\omega_0$, a regime in which Sec. VI predicts that the thermal toll removes net harvesting at strong coupling.

Extraction in place. The local unitary of Sec. VI E must be short compared with $1/\lambda_{rc}$, i.e. it requires a Rabi frequency well above $\lambda_{rc}/2\pi = 0.25$–1.5 GHz. This is comparable to or larger than the anharmonicity of a transmon, a few hundred megahertz [60], so that leakage out of the qubit subspace sets the limit. In-place extraction is therefore most demanding exactly where it pays most: its advantage over decoupling is negligible at weak coupling and large only at $\lambda_{rc} \gtrsim 0.2\,\omega_0$ (Sec. VI E). In this regime the decoupling ramp is the more practical route.

Observables. Three predictions can be tested with qubit readout alone, using a separate dispersive readout resonator after the battery has been disconnected. (i) The ergotropy that survives decoupling, including its coherent part, follows from state tomography of the battery qubit, as in the demonstration of coherent-ergotropy extraction on a superconducting processor [8]. Scanning the start time and duration of the ramp maps the recovered fraction of Fig. 5(a) and tests the harvesting criterion (19). (ii) The spectral origin of the gain (Sec. IV) can be tested by detuning a frequency-tunable resonator from the qubit at fixed κ, which keeps the memory time but removes the spectral weight at ω_0; tuning a flux-tunable qubit instead is equivalent up to the accompanying change of λ_{rc}/ω_0. A detuning of 20–40% at $\lambda_{rc} = 0.05\,\omega_0$ and $\kappa/2\pi = 50$ MHz reduces the gain from 82 to 0.86–0.95 of the Markovian value [Fig. 3(b)]. (iii) The diabatic part of the toll is left behind as correlated qubit–photon excitations. In the closed single-mode theory of Eq. (22), the energy that a ramp fails to return, $E_b|F(\nu)|^2$, is carried by pairs $|g,0\rangle \to |e,1\rangle$ of energy $\omega_0+\omega_r$, so that a qubit decoupled from its dressed ground state is found excited with probability

$$P_{\mathrm{pair}}(\tau) = \left(\frac{\lambda_{rc}}{\omega_0+\omega_r}\right)^2 |F(\nu)|^2. \tag{26}$$

For sudden decoupling, $|F|^2 = 1$, this is 2.3% at $\lambda_{rc} = 0.3\,\omega_0$ and 0.25% at $0.1\,\omega_0$ (Table I), well above the thermal excited-state population at 20 mK ($e^{-\omega_0/T} \approx 6\times10^{-6}$), and it vanishes at the ramp durations τ_k of Eq. (23), smeared by the bath width (Sec. VI). Because the qubit retains this excitation long after the photon has leaked into the line, the binding energy and its finite-time removal become directly measurable.

The same criteria apply to other platforms. *Organic microcavities* operate at room temperature but at optical frequencies, so that again $T \ll \omega_0$ [10]. Their structured environments are vibrational, and the relevant criterion is that of Sec. IV: the gain requires vibronic spectral weight at the battery frequency, not a long vibrational memory. *Spin-based batteries* and other low-frequency platforms operate at $T \gtrsim \omega_0$. There, zero-temperature solutions overestimate the stored work by factors of about three, the toll approaches $2\lambda_{rc}^2$ while the revival falls below 30% of its zero-temperature value, and net harvesting of revivals is not expected.

VIII. DISCUSSION

Table II summarizes how the main claims about open quantum batteries fare against exact dynamics. Two of them survive, with corrections in size. The revival of stored ergotropy in a structured bath is physical, and

TABLE II. Claims about open quantum batteries tested against numerically exact dynamics. Numbers refer to the models and parameter ranges of Sec. II.

Claim	Refs.	Exact result
Environmental memory revives the stored ergotropy and enables charging that the Markovian limit forbids (single channel)	[14, 15]	Confirmed at $T \lesssim 0.1\,\omega_0$; rotating-wave solutions accurate to 8.4% for $r < 1$ up to $\lambda_{rc} = 0.3\,\omega_0$. Zero-temperature results overestimate storage by factors of 1.4–3.2 at $T = 0.5$–$1\,\omega_0$ (Sec. III).
Strong collective coupling charges a battery through a shared bath	[16, 21, 22]	Not confirmed beyond $\lambda_{rc} \approx 0.1\,\omega_0$: peak ergotropy overestimated by factors of 1.3–1.7 at $\lambda_{rc} = 0.2$ and 27.5 at $\lambda_{rc} = 0.3$ (energy: 33%). Dark-state trapping survives (Sec. III).
The Bloch–Redfield equation describes strongly coupled non-Markovian batteries	[29–31]	Uncontrolled for $r < 1$: storage underestimated by 80–98.5%, peak charged ergotropy overestimated by up to a factor of 43.5 (energy: 69%), positivity violated for slow baths (Secs. III and IV).
Memory (non-Markovianity) is the resource	[14, 15, 17, 18]	Not confirmed: information backflow does not predict the gain. Detuned peaks with long memory and $\mathcal{N}_{\mathrm{BLP}}$ up to 2.3 give 0.85–0.95 of the Markovian value; slow Drude–Lorentz baths give 0.45–0.74. The gain (up to 82) requires spectral weight at ω_0 (Sec. IV).
The ergotropy of the coupled battery measures the stored work	implicit in the above	In place, yes: the local ergotropy agrees with it to within -2% to $+9\%$ ($\varphi = 0$). After disconnection, no: with the best ramp tested, 61% of the first revival is recovered at $\lambda_{rc} = 0.3$, $r = 0.2$, $T = 0.1\,\omega_0$, and none at $T = 0.5\,\omega_0$ (Sec. VI).
The Hamiltonian of mean force defines the energy of a strongly coupled system	[38, 40]	As a battery-energy operator it fails: mean-force ergotropy vanishes as $T \to 0$ for every state ($0.19\,\mathcal{E}$ at $T = 0.05\,\omega_0$, $\lambda_{rc} = 0.3$); undefined for the non-ergodic shared bath (Sec. V).

the rotating-wave solutions that predict it are quantitatively reliable for single-channel protocols at low temperature. The others do not survive in their stated form. The large charging peaks predicted for strong collective coupling are artifacts of the rotating-wave approximation, second-order master equations cannot decide the question in the regime where it is posed, and memory alone is not a resource. Most importantly, the figure of merit used throughout the field, the ergotropy of the coupled battery, is a good estimate of the work that can be withdrawn in place. Whenever the battery must be disconnected, however, it omits a cost of the same order as the effect it measures.

The decoupling toll closes the energy budget of a strongly coupled battery. Connecting a battery to a thermal bath is free, because $\langle H_I \rangle = \langle Q \rangle \langle X \rangle_{\mathrm{th}} = 0$ for a product state, so the toll is the full interaction cost of a storage cycle. For batteries charged by thermalization, Refs. [36, 37, 59] showed numerically that the connection and disconnection work limits the efficiency of a charging cycle. Equations (10)–(12) give this cost in closed form for a qubit, for any spectral density and temperature, and Eq. (19) extends it to dynamical revivals far from equilibrium. The same structure, a counter-rotating binding energy, a resonant thermal term and a static polaron term, applies to any two-level device that is coupled to and disconnected from a bosonic environment. This includes the strokes of strongly coupled heat engines and the readout of quantum sensors. The $\cos^2$ ramp of Eq. (22) complements numerical optimal-control approaches to work minimization in strongly coupled systems [66, 67]. It provides an analytic protocol that approaches the adiabatic bound to within the bath width after a few battery periods, and a benchmark against which numerically optimized ramps can be measured. Decoupling is not the only route to the stored energy: local unitaries applied while the battery remains coupled extract the local ergotropy, which can exceed the switch-off value [33–35]. For the storage protocol it exceeds the best ramped net work at every point we computed (Sec. VI E). The toll and the decoupling ramp are therefore the relevant theory whenever the application requires disconnection.

Section VII translates these results into requirements for superconducting, molecular and spin-based platforms.

The analytic results have a well-defined range of validity, which we summarize in Table III. The toll is a second-order result, and its corrections scale as λ_{rc}^4; they reach 6% at $\lambda_{rc} = 0.3\,\omega_0$ (7% for the ramp work). The revival theory assumes a resonant bath mode and, for $\varphi \neq 0$, is limited to $\lambda_{rc} \leq 0.2$. Beyond this, the transient toll becomes non-perturbative and must be computed numerically. We have treated up to three battery cells and ideal unitary extraction. All open-system dynamics quoted in the text are computed with HEOM. The closed

single-mode ramp (Fig. 5(b)), the rotating-wave analysis of the thermal revival and the polaron model are separate model calculations and are identified as such, and equilibrium tolls are also compared with the system–RC Gibbs state. The reaction-coordinate model with a Markovian residual bath reproduces the figures of merit but not the interaction energy at strong coupling (Appendix A).

IX. CONCLUSION

We have tested the non-Markovian advantage of open quantum batteries with numerically exact dynamics, across three protocols, four families of spectral densities and collective batteries of up to three cells, and have derived in closed form the work needed to disconnect a strongly coupled qubit battery. Exact solutions exist for harmonic batteries in quantum Brownian motion [68] and for spin baths [18]; we are not aware of a previous test of the claimed non-Markovian advantage against numerically exact dynamics for structured bosonic baths, or of a closed-form expression for the cost of withdrawing it from a qubit battery.

- The rotating-wave, zero-temperature and Redfield treatments that underlie the literature fail in identifiable regions, overestimating the charged ergotropy by factors of up to 27.5 and 43.5 near the passivity threshold (the charged energy by up to 69%) and the stored work at $T = \omega_0$ by factors of 2.6–3.2.

- The gain originates from spectral weight at the battery frequency, not from memory, and information backflow does not predict it. Baths with long memory and strong information backflow but no such weight reduce the stored work to 0.45–0.95 of the Markovian value, whereas resonant peaked baths raise it up to 82-fold.

- The decoupling toll obeys $W_{\rm eq} = \cos^2\varphi\,[W_{\rm CR} + W_{\rm res}(T)] + \sin^2\varphi\, W_z$ to within 7%. In second-order theory, a revival yields net work after disconnection only if it exceeds the binding energy, half the sudden toll, and a $\cos^2$ ramp lasting a few battery periods nearly reaches this bound. A fast local unitary applied in place avoids the toll and outperforms every decoupling protocol we tested. In collective batteries the toll per cell exceeds its second-order value, by a factor of 1.9 for three cells at $\lambda_{rc} = 0.3\,\omega_0$.

These results give an operational answer to the long-standing question of how to define work at strong coupling. Mean-force ergotropy collapses at low temperature. The meaningful quantities are the local ergotropy for a battery used in place, which the coupled-state ergotropy approximates closely, and the net work after disconnection, which can be predicted and optimized analytically. Designs that require the battery to be disconnected but are optimized for the ergotropy of the coupled battery will overestimate the deliverable work by 60% at $T = 0.1\,\omega_0$ even with the best ramp we tested, and by a factor of four with sudden decoupling, as at $\lambda_{rc} = 0.3\,\omega_0$, $r = 0.2$; at $T = 0.5\,\omega_0$ the same revival yields no net work at all. A non-perturbative theory of the transient toll for tilted coupling, the extension to larger collective batteries, where the toll per cell grows beyond second order, and a demonstration of the decoupling ramp on a superconducting platform are the next steps. More broadly, every quantum device that must be connected to and disconnected from a structured environment, from batteries to heat engines and sensors, pays this toll, and the criterion derived here provides a benchmark for claims of quantum thermodynamic advantage at strong coupling.

DATA AVAILABILITY

The data that support the findings of this article are publicly available [69]. They were generated by numerical simulations. The source code and parameters used to generate the simulations, the numerical results underlying Figs. 1–6 and Tables I–IV, the convergence tests of Appendix A and the scripts that produce the figures are publicly available from the same repository [69]. The simulations use the open-source package QuTiP, version 5.2.3 [46, 70].

Appendix A: Numerical convergence

Settings. All HEOM calculations use QuTiP-BoFiN [46] with an adaptive integrator (absolute and relative tolerances 10^{-9} and 10^{-7}) and output every $0.25/\omega_0$. Underdamped baths are expanded with $N_k = 3$ Matsubara terms. The default hierarchy depth is 6 for $\lambda_{rc} \le 0.05$, 8 for $\lambda_{rc} \le 0.1$ or $T < 0.3\,\omega_0$, and 12 otherwise. For overdamped Brownian baths ($r = 5$, i.e., $\kappa \ge 2\omega_r$), where the analytic Matsubara decomposition does not apply, $C(t)$ is fitted on $t \in [0, 30]/\omega_0$ with two to four exponentials for each of its real and imaginary parts (target root-mean-square error 10^{-6}), at depth 6. Drude–Lorentz baths use Padé expansions with $N_k = 3$ ($\gamma \le \omega_0$) or $N_k = 6$ ($\gamma = 5\,\omega_0$) at depth 8, except for $\gamma = 5\,\omega_0$ at $T = 0.1\,\omega_0$, where the Padé hierarchy is unstable and a fit of $C(t)$ on $[0, 40]/\omega_0$ is used instead. Ohmic baths use such fits at depth 6 (storage) or 5 (charging). The RC model (6) uses a Fock cutoff of 14.

Tests. Table IV lists the change of the figure of merit when N_k, the depth or the Fock cutoff is increased, for the most demanding points of each family: strong coupling, slow baths and high temperature. The default settings meet the 1% criterion of Sec. II for storage and charger-mediated charging through underdamped baths at $T \le 0.5\,\omega_0$, for broad Drude–Lorentz and Ohmic

TABLE III. Accuracy of the analytic results against exact dynamics. Net work is given in units of ω_0.

Quantity	Accuracy	Range
$W_{\rm eq}$, Eqs. (10)–(12)	$\leq 7\%$	$T \leq 2\,\omega_0$, $\varphi \leq \pi/4$, $\lambda_{rc} \leq 0.3$; UD ($\kappa \ll \omega_0$), DL, Ohmic
$\omega_{\rm eff}$, Eq. (14)	$\leq 1\%$	$T \leq 0.1\,\omega_0$
$W(\tau)$, Eq. (22)	$\leq 0.7\%$ (λ_{rc}=0.1), $\leq 7\%$ (λ_{rc}=0.3)	closed single mode
$\mathcal{E}_n$, Eqs. (17), (24)	$\leq 3\%$ ($\lambda_{rc}\leq$0.2), $\leq 8\%$ (0.3)	$\varphi = 0$, $T \leq 0.5\,\omega_0$
$\mathcal{E}_n$, polaron	$\leq 6\%$	$\lambda_{rc} \leq 0.2$, $\varphi = \pi/8, \pi/4$
$\mathcal{E}_n^{\rm net}$, Eq. (19)	≤ 0.009 (T=0.1), ≤ 0.007 (T=0.5)	$\varphi = 0$, $\lambda_{rc} \leq 0.3$
$\mathcal{E}_n^{\rm net}$, $\varphi = \pi/4$	≤ 0.014 (revival from dynamics)	$\lambda_{rc} = 0.2$, $r = 0.05$

baths, and for the equilibrium toll. Four regimes need deeper hierarchies, and for them we use the deepest values in Table IV:

- *shared-bath charging at strong coupling* ($\lambda_{rc} = 0.3$, $r = 0.2$, $T = 0.1\,\omega_0$), where depth 8 underestimates the peak battery ergotropy by 25% and depths 12 and 14 agree to within 0.4%;
- *shared-bath charging at finite temperature*, where depth 6 underestimates the peak by 1.4% ($T = 0.5\,\omega_0$) and 21% ($T = \omega_0$), and the successive changes from depth 10 to 12 and from 12 to 14 at $T = \omega_0$ are 2.8% and 0.7%;
- *storage at* $T = \omega_0$, where depth 6 overestimates the time-integrated ergotropy by 4% and the overdamped bath at depth 6 underestimates it by 2.2%;
- *slow Drude–Lorentz baths at* $T = 0.5\,\omega_0$, where depth 8 underestimates the stored work by up to 4.5% and the peak charge by 8.9%, and depths 12 and 16 (14 for charging) agree to within about 1%.

The residual uncertainty of the values used is therefore below 1% almost everywhere. The exceptions are shared-bath charging at $T = \omega_0$ and charging through the slow Drude–Lorentz bath at $T = 0.5\,\omega_0$, where we estimate it at 1% from the decreasing sequence of increments. The shared-bath hierarchy is numerically unstable at $\lambda_{rc} = 0.3$, $r = 0.05$, $T = 0.1\,\omega_0$ (the battery ergotropy diverges at depths 8 and 12) and, for all Drude–Lorentz runs with $\gamma = 5\,\omega_0$, at $T = 0.1\,\omega_0$ (divergence or integrator failure with both Padé and fitted expansions). We exclude these points. For collective storage the hierarchy is likewise unstable for the narrowest bath ($r = 0.05$) at $N = 2$, $\lambda_{rc} = 0.3$ and $N = 3$, $\lambda_{rc} = 0.2$; for $N = 3$, $\lambda_{rc} = 0.3$, $r = 0.2$ it is unstable at depth 12; at depths 14 and 16 the results agree to 0.2% and the long-time toll agrees with the system–RC Gibbs value to 0.1%.

Decoupling toll. The interaction energy obtained from the first-tier auxiliary density operators [Eq. (8)] reproduces the interaction energy $\lambda_{rc}\langle Q(a+a^\dagger)\rangle$ of the system–RC Gibbs state to 1–2 $\times\, 10^{-4}$ at $T = 0.5\,\omega_0$ and 0.4% at $T = 0.2\,\omega_0$ (HEOM steady states, $\lambda_{rc} = 0.1$–0.2, $r = 0.05$), and the HEOM steady-state toll changes by less than 10^{-7} when the depth is increased (Drude–Lorentz, $\gamma = 0.2$ and $5\,\omega_0$).

Reaction coordinate. Increasing the Fock cutoff from 14 to 24 changes the RC figures of merit by less than 3×10^{-6} at the most demanding points ($\lambda_{rc} = 0.2$–0.3, T up to ω_0). The remaining difference from HEOM therefore stems from the Born–Markov treatment of the residual bath in Eq. (6), which thermalizes the bare rather than the dressed reaction coordinate, and from the initial state of the reaction coordinate. For the figures of merit at $T \leq 0.5\,\omega_0$ and $r \leq 1$ the difference has a median of 0.2% and is below 4% for 58 of 65 points, with the largest deviations for shared-bath charging at strong coupling (up to a factor of 2.2 at $\lambda_{rc} = 0.3$, $r = 0.2$). The interaction energy is more sensitive: at $\lambda_{rc} = 0.3$, $r = 0.2$ the RC model gives a long-time toll of $0.102\,\omega_0$ at $T = 0.5\,\omega_0$, against $0.143\,\omega_0$ from HEOM and from the system–RC Gibbs state, and a sudden-decoupling net work of $0.006\,\omega_0$ at $T = 0.1\,\omega_0$, against $0.022\,\omega_0$ from HEOM. All open-system decoupling and local-ergotropy results are therefore computed with HEOM; the closed single-mode ramp of Fig. 5(b) is a separate model calculation.

Time-dependent coupling. Integrating $\mathcal{L}_0 + \mathcal{L}_1$ reproduces the standard HEOM propagation to 10^{-7} in the state, and the hierarchy built for $3Q$ equals $\mathcal{L}_0 + 3\mathcal{L}_1$ to machine precision, confirming the linear decomposition used for the ramps. For the long ramps of Sec. VII ($\omega_0\tau = 10\pi$, $\lambda_{rc} = 0.1$, $r = 0.05$, $T = 0.1\,\omega_0$), increasing the depth from 8 to 10 or doubling the number of time points in the work integral changes the net work by less than $10^{-5}\,\omega_0$, and the values at $\omega_0\tau \leq 8$ reproduce those of Fig. 5 to within $10^{-6}\,\omega_0$.

All tests are reproduced by the scripts `conv_check.py`, `conv_check2.py`–`conv_check4.py`, `rc_cutoff.py`, `rc_vs_heom.py`, `hi_check.py`, `decouple_heom_conv.py`, `ramp_long.py` and `ncell_conv.py` in the accompanying code, which write the results to the data files listed there.

TABLE IV. Convergence of the HEOM and RC figures of merit (storage: $\int \mathcal{E}\, dt$; charging: $\max_t \mathcal{E}_B$). Relative changes refer to the more converged value; "0" means that both settings give no charging; "both" denotes storage and charger-mediated charging. Successive refinements are separated by commas.

Bath	Protocol	Parameters	Refinement	Relative change
UD (Matsubara)	storage	$\lambda_{rc} = 0.2, 0.3$; $r = 0.05$–1; $T = 0.1$	depth $8 \to 12$	$< 5 \times 10^{-5}$
	storage	$\lambda_{rc} = 0.3$; $r = 0.05, 0.2$; $T = 0.1$	N_k $3 \to 5$	0.2–0.4%
	storage	$\lambda_{rc} = 0.05$; $r = 0.05$; $T = 0.1, 0.5$	depth $6 \to 10$	0.06%, 0.3%
	storage	$\lambda_{rc} = 0.02, 0.05$; $r = 0.05$; $T = 1$	depth 6→10→12→14	4%, $< 0.1\%$, $< 0.1\%$
	storage	$\lambda_{rc} = 0.1$; $r = 0.05$; $T = 1$	depth $8 \to 12$	0.6%
	storage	$\lambda_{rc} = 0.3$; $r = 0.2$; $T = 1$	depth $12 \to 14$	$< 10^{-5}$
	charger	all points of the storage tests	depth, N_k	$< 2 \times 10^{-5}$ or 0
	shared	$\lambda_{rc} = 0.05$; $r = 0.05$; $T = 0.1$	depth $6 \to 10$	$< 10^{-4}$
	shared	$\lambda_{rc} = 0.2$; $r = 0.05, 0.2$; $T = 0.1$	depth $8 \to 12$	$< 0.1\%$
	shared	$\lambda_{rc} = 0.3$; $r = 0.2$; $T = 0.1$	depth 8→12→14	25%, 0.4%
	shared	$\lambda_{rc} = 0.3$; $r = 0.05$; $T = 0.1$	depth 8, 12	unstable (excluded)
	shared	$\lambda_{rc} = 0.02, 0.05$; $r = 0.05$; $T = 0.5$	depth 6→10	1.4%
	shared	$\lambda_{rc} = 0.05$; $r = 0.05$; $T = 0.5$	depth 10→12→14	$< 0.1\%$, $< 0.01\%$
	shared	$\lambda_{rc} = 0.02, 0.05$; $r = 0.05$; $T = 1$	depth 6→10→12→14	21%, 2.8%, 0.7%
UD (fit)	storage	$\lambda_{rc} = 0.3$; $r = 5$; $T = 0.1, 0.5$	depth 6→9→12	$< 10^{-4}$; 0.25%, 0.05%
	storage	$\lambda_{rc} = 0.3$; $r = 5$; $T = 1$	depth 6→9→12	2.2%, 0.25%
	charger	$\lambda_{rc} = 0.3$; $r = 5$; $T = 0.1$	depth $6 \to 9$	$< 10^{-5}$
DL (Padé)	both	$\lambda_{\mathrm{DL}} = 0.1$; $\gamma = 0.05$; $T = 0.1$	depth $8 \to 12$	$< 0.04\%$
	storage	$\lambda_{\mathrm{DL}} = 0.01, 0.03, 0.1$; $\gamma = 0.05$; $T = 0.5$	depth 8→12→16	$\leq 4.5\%$, $\leq 0.8\%$
	storage ($\varphi = \pi/4$)	$\lambda_{\mathrm{DL}} = 0.1$; $\gamma = 0.05$; $T = 0.5$	depth 8→12→16	2.3%, 0.3%
	charger	$\lambda_{\mathrm{DL}} = 0.1$; $\gamma = 0.05$; $T = 0.5$	depth 8→12→14	8.9%, 1.0%
	storage	$\lambda_{\mathrm{DL}} = 0.1$; $\gamma = 0.2, 1$; $T = 0.5$	depth $8 \to 12$	$< 0.1\%$
	both	$\lambda_{\mathrm{DL}} = 0.1$; $\gamma = 5$ ($N_k = 6$); $T = 0.5$	depth $8 \to 11$	$\approx 0.1\%$
Ohmic (fit)	both	$\alpha = 0.05$; $(\omega_c, T) = (1, 0.1), (5, 0.5)$	depth $+3$	$< 10^{-5}$
DL (Padé)	W_{eq} (steady state)	$\lambda_{\mathrm{DL}} = 0.1$; $\gamma = 0.2, 5$; $T = 0.5$	depth $+3$, $+2$	$< 10^{-7}$
RC	all	$\lambda_{rc} = 0.2, 0.3$; $T = 0.1$–1 (6 points)	Fock $14 \to 24$	$< 3 \times 10^{-6}$
UD	ramp, $\mathcal{E}_{\mathrm{loc}}$	$\lambda_{rc} = 0.2, 0.3$; $r = 0.05, 0.2$; $T = 0.1, 0.5$	depth 8→11, 12→14	$< 10^{-4}$
UD, N cells	storage	$(N, \lambda_{rc}) = (2, 0.3), (3, 0.2)$; $r = 0.2$	depth 12→14, 10→12	$< 10^{-3}$, 0.16%
	storage	$(3, 0.3)$; $r = 0.2$	depth 12→14→16	12 unstable; 0.2%
	storage	$(2, 0.2)$; $r = 0.05$; $t \leq 60$	depth 9→11	0.1%
	storage	$(N, \lambda_{rc}) = (2, 0.3), (3, 0.2)$; $r = 0.05$	depth ≤ 12	unstable (excluded)

[1] A. E. Allahverdyan, R. Balian, and T. M. Nieuwenhuizen, Maximal work extraction from finite quantum systems, Europhys. Lett. **67**, 565 (2004).

[2] R. Alicki and M. Fannes, Entanglement boost for extractable work from ensembles of quantum batteries, Phys. Rev. E **87**, 042123 (2013).

[3] F. C. Binder, S. Vinjanampathy, K. Modi, and J. Goold, Quantacell: powerful charging of quantum batteries, New J. Phys. **17**, 075015 (2015).

[4] D. Ferraro, M. Campisi, G. M. Andolina, V. Pellegrini, and M. Polini, High-power collective charging of a solid-state quantum battery, Phys. Rev. Lett. **120**, 117702 (2018).

[5] F. Campaioli, S. Gherardini, J. Q. Quach, M. Polini, and G. M. Andolina, Colloquium: Quantum batteries, Rev. Mod. Phys. **96**, 031001 (2024).

[6] S. Campbell, I. D'Amico, M. A. Ciampini, J. Anders, N. Ares, *et al.*, Roadmap on quantum thermodynamics, Quantum Sci. Technol. **11**, 012501 (2026), arXiv:2504.20145.

[7] C.-K. Hu, C. Liu, J. Zhao, L. Zhong, Y. Zhou, M. Liu, H. Yuan, Y. Lin, Y. Xu, G. Hu, G. Xie, Z. Liu, R. Zhou, Y. Ri, W. Zhang, R. Deng, A. Saguia, X. Linpeng, M. S. Sarandy, S. Liu, A. C. Santos, D. Tan, and D. Yu, Quantum charging advantage in superconducting solid-state batteries, Physical Review Letters **136**, 060401 (2026), arXiv:2602.08610.

[8] L. Li, S. Zhao, Y.-H. Shi, K. Xu, H. Fan, D. Zheng, and Z. Xiang, Experimental extraction of coherent ergotropy and its energetic cost in a superconducting qubit, Phys.

Rev. Research **7**, 043236 (2025), arXiv:2506.16881.
[9] J. Zhang, P. Wang, W. Chen, Z. Cai, M. Qiao, R. Li, Y. Huang, H. Tian, C. Luan, H. Tu, K. Cui, L. Yan, J. Zhang, J. Zhang, M. Yung, and K. Kim, Single-ion information engine for charging quantum battery, Physical Review Letters **135**, 140403 (2025), arXiv:2408.14373.
[10] K. Hymas, J. B. Muir, D. Tibben, J. van Embden, T. Hirai, C. J. Dunn, D. E. Gómez, J. A. Hutchison, T. A. Smith, and J. Q. Quach, Experimental demonstration of a scalable room-temperature quantum battery, Light Sci. Appl. **15**, 168 (2026), arXiv:2501.16541.
[11] H.-X. Gao, X.-C. Zhuang, Q.-F. Xue, Q. Zhang, Y.-J. Zhang, Y.-J. Xia, and Z.-X. Man, Experimental extraction and dynamics of ergotropy in open quantum systems, Physical Review A **113**, 052210 (2026).
[12] S. Pal, K. Hovhannisyan, O. Porat, S. Dutta, J. Anders, and H. Knowles, Ancilla mediated steady-state engineering in open quantum systems, arXiv e-prints 10.48550/arXiv.2609.04905 (2026), arXiv:2609.04905.
[13] W.-L. Song, J.-L. Wang, B. Zhou, W.-L. Yang, and J.-H. An, Self-discharging mitigated quantum battery, Physical Review Letters **135**, 020405 (2025), arXiv:2504.01679.
[14] F. H. Kamin, F. T. Tabesh, S. Salimi, F. Kheirandish, and A. C. Santos, Non-Markovian effects on charging and self-discharging process of quantum batteries, New J. Phys. **22**, 083007 (2020).
[15] J. L. Li, H. Z. Shen, and X. X. Yi, Quantum batteries in non-markovian reservoirs, Optics Letters **47**, 5614 (2022).
[16] F. T. Tabesh, F. H. Kamin, and S. Salimi, Environment-mediated charging process of quantum batteries, Physical Review A **102**, 052223 (2020), arXiv:2005.12823.
[17] A. Oularabi, A. El Allati, and K. El Anouz, Enhancing ergotropy of quantum batteries through coherence and non-markovianity, Physica A Statistical Mechanics and its Applications **679**, 131003 (2025).
[18] J.-K. Xu, J.-B. You, and W.-L. Yang, Non-Markovian-assisted advantage for central-spin quantum battery, Phys. Rev. A **113**, 032202 (2026).
[19] Y. Wang and J. Jin, Early-stage memory effect on the dephasing charger-mediated quantum battery, Physical Review A **114**, 032407 (2026), arXiv:2602.14146.
[20] M. H. Barati Farimani and A. Mortezapour, Detuning-controlled phase transition from passive to active regimes in non-Markovian quantum batteries (2026), arXiv:2604.09888.
[21] M.-L. Hu, T. Gao, and H. Fan, Efficient wireless charging of a quantum battery, Phys. Rev. A **111**, 042216 (2025), arXiv:2501.08843.
[22] J.-J. Jiang, J.-D. Cao, Y.-F. Zhang, M.-L. Song, and D. Wang, Quantum coherence and entanglement in wireless quantum batteries, Phys. Rev. A **114**, 022420 (2026), arXiv:2607.27718.
[23] Z.-G. Lu, G. Tian, X.-Y. Lü, and C. Shang, Topological quantum batteries, Physical Review Letters **134**, 180401 (2025), arXiv:2405.03675.
[24] I. Medina, O. Culhane, F. C. Binder, G. T. Landi, and J. Goold, Anomalous discharging of quantum batteries: The ergotropic mpemba effect, Physical Review Letters **134**, 220402 (2025), arXiv:2412.13259.
[25] Y. Li, W. Li, and X. Li, Ergotropic mpemba effect in non-markovian quantum systems, Physical Review A **112**, 032209 (2025).
[26] G. Francica, F. C. Binder, G. Guarnieri, M. T. Mitchison, J. Goold, and F. Plastina, Quantum coherence and ergotropy, Phys. Rev. Lett. **125**, 180603 (2020).
[27] B. M. Garraway, Nonperturbative decay of an atomic system in a cavity, Phys. Rev. A **55**, 2290 (1997).
[28] B. Bellomo, R. Lo Franco, and G. Compagno, Non-Markovian effects on the dynamics of entanglement, Phys. Rev. Lett. **99**, 160502 (2007).
[29] S.-C. Zhao, Z.-R. Zhao, and N.-Y. Zhuang, Non-Markovian N-spin chain quantum battery in thermal charging process, Phys. Rev. E **112**, 024129 (2025), arXiv:2504.05348.
[30] S.-C. Zhao, Y.-F. Yang, and N.-Y. Zhuang, Rapid and stable collective charging and discharge suppression in strongly coupled many-body quantum batteries, arXiv e-prints 10.48550/arXiv.2502.08665 (2025), arXiv:2502.08665.
[31] Y.-F. Yang and S.-C. Zhao, Charging dynamics in a distance-modulated planar quantum-battery architecture, arXiv e-prints 10.48550/arXiv.2604.22878 (2026), arXiv:2604.22878.
[32] Z.-Y. Peng, S.-C. Zhao, L. Luo, and N.-Y. Zhuang, Energy-invariant catalysis of stable ergotropy in strongly coupled spin-chain quantum batteries, Physica A **689**, 131462 (2026), arXiv:2508.02772.
[33] R. Salvia, G. De Palma, and V. Giovannetti, Optimal local work extraction from bipartite quantum systems in the presence of Hamiltonian couplings, Phys. Rev. A **107**, 012405 (2023), arXiv:2206.14842.
[34] R. Castellano, D. Farina, V. Giovannetti, and A. Acin, Extended local ergotropy, Physical Review Letters **133**, 150402 (2024), arXiv:2401.10996.
[35] G. Di Bello, D. Farina, D. Jansen, C. A. Perroni, V. Cataudella, and G. De Filippis, Local ergotropy and its fluctuations across a dissipative quantum phase transition, Quantum Science and Technology **10**, 015049 (2025), arXiv:2408.02655.
[36] K. V. Hovhannisyan, F. Barra, and A. Imparato, Charging assisted by thermalization, Phys. Rev. Research **2**, 033413 (2020).
[37] D. Feliú and F. Barra, System-bath correlations and finite-time operation enhance the efficiency of a dissipative quantum battery, Quantum Science and Technology **9**, 035043 (2024), arXiv:2403.08573.
[38] P. Talkner and P. Hänggi, Colloquium: Statistical mechanics and thermodynamics at strong coupling: Quantum and classical, Rev. Mod. Phys. **92**, 041002 (2020).
[39] J. D. Cresser and J. Anders, Weak and ultrastrong coupling limits of the quantum mean force Gibbs state, Phys. Rev. Lett. **127**, 250601 (2021).
[40] N. Pathania, D. Tiwari, and S. Banerjee, Quantum thermodynamics of open quantum systems: Nature of thermal fluctuations, Quantum Inf. Process. **24**, 290 (2025), arXiv:2407.21584.
[41] D. Tiwari, B. Bose, and S. Banerjee, Strong coupling non-Markovian quantum thermodynamics of a finite-bath system, J. Chem. Phys. **162**, 114104 (2025), arXiv:2404.15915.
[42] I. González, S. Chakraborty, and Á. Rivas, Intrinsic Hamiltonian of mean force and strong-coupling quantum thermodynamics (2025), arXiv:2506.02888.
[43] J. Jin, Temperature–Hamiltonian ambiguity in strong-coupling quantum equilibrium (2026), arXiv:2609.33389.
[44] Y. Tanimura and R. Kubo, Time evolution of a quan-

tum system in contact with a nearly Gaussian-Markoffian noise bath, J. Phys. Soc. Jpn. **58**, 101 (1989).
[45] Y. Tanimura, Numerically "exact" approach to open quantum dynamics: The hierarchical equations of motion (HEOM), J. Chem. Phys. **153**, 020901 (2020).
[46] N. Lambert, T. Raheja, S. Cross, P. Menczel, S. Ahmed, A. Pitchford, D. Burgarth, and F. Nori, QuTiP-BoFiN: A bosonic and fermionic numerical hierarchical-equations-of-motion library with applications in light-harvesting, quantum control, and single-molecule electronics, Phys. Rev. Research **5**, 013181 (2023).
[47] J. Iles-Smith, N. Lambert, and A. Nazir, Environmental dynamics, correlations, and the emergence of noncanonical equilibrium states in open quantum systems, Phys. Rev. A **90**, 032114 (2014).
[48] P. Strasberg, G. Schaller, N. Lambert, and T. Brandes, Nonequilibrium thermodynamics in the strong coupling and non-Markovian regime based on a reaction coordinate mapping, New J. Phys. **18**, 073007 (2016).
[49] M. Shubrook, J. Iles-Smith, and A. Nazir, Non-Markovian quantum heat statistics with the reaction coordinate mapping, Quantum Sci. Technol. **10**, 025063 (2025), arXiv:2408.08829.
[50] D. Tamascelli, A. Smirne, S. F. Huelga, and M. B. Plenio, Nonperturbative treatment of non-Markovian dynamics of open quantum systems, Phys. Rev. Lett. **120**, 030402 (2018).
[51] F. Albarelli, B. Vacchini, and A. Smirne, Pseudomode treatment of strong-coupling quantum thermodynamics, Quantum Sci. Technol. **10**, 015041 (2024).
[52] A. Strathearn, P. Kirton, D. Kilda, J. Keeling, and B. W. Lovett, Efficient non-Markovian quantum dynamics using time-evolving matrix product operators, Nat. Commun. **9**, 3322 (2018).
[53] M. Shubrook, M. Cygorek, E. Gauger, J. Iles-Smith, and A. Nazir, Numerically exact open quantum system work statistics with process tensors (2025), arXiv:2512.16823.
[54] H. M. Rizvi, D. Tiwari, and S. Banerjee, Two-qubit spin-boson model in the strong coupling regime: Coherence, non-Markovianity, and quantum thermodynamics (2026), arXiv:2601.15026.
[55] T. Z. Jawad, Ergotropy protection via cavity detuning in collective open quantum batteries (2026), arXiv:2605.04042.
[56] B. Ahmadi, A. Balaji Ravichandran, P. Mazurek, S. Barzanjeh, and P. Horodecki, Harnessing environmental noise for quantum energy storage, arXiv e-prints 10.48550/arXiv.2510.06384 (2025), arXiv:2510.06384.
[57] H.-P. Breuer, E.-M. Laine, and J. Piilo, Measure for the degree of non-Markovian behavior of quantum processes in open systems, Phys. Rev. Lett. **103**, 210401 (2009).
[58] S. Wißmann, A. Karlsson, E.-M. Laine, J. Piilo, and H.-P. Breuer, Optimal state pairs for non-Markovian quantum dynamics, Phys. Rev. A **86**, 062108 (2012).
[59] M. Araya Satriani and F. Barra, Daemonic quantum battery charged by thermalization, Quantum Sci. Technol. **9**, 045035 (2024), arXiv:2405.15949.
[60] J. Koch, T. M. Yu, J. Gambetta, A. A. Houck, D. I. Schuster, J. Majer, A. Blais, M. H. Devoret, S. M. Girvin, and R. J. Schoelkopf, Charge-insensitive qubit design derived from the Cooper pair box, Phys. Rev. A **76**, 042319 (2007).
[61] T. Niemczyk, F. Deppe, H. Huebl, E. P. Menzel, F. Hocke, M. J. Schwarz, J. J. Garcia-Ripoll, D. Zueco, T. Hümmer, E. Solano, A. Marx, and R. Gross, Circuit quantum electrodynamics in the ultrastrong-coupling regime, Nat. Phys. **6**, 772 (2010).
[62] F. Yoshihara, T. Fuse, S. Ashhab, K. Kakuyanagi, S. Saito, and K. Semba, Superconducting qubit–oscillator circuit beyond the ultrastrong-coupling regime, Nat. Phys. **13**, 44 (2017).
[63] P. Forn-Díaz, L. Lamata, E. Rico, J. Kono, and E. Solano, Ultrastrong coupling regimes of light-matter interaction, Rev. Mod. Phys. **91**, 025005 (2019).
[64] A. Frisk Kockum, A. Miranowicz, S. De Liberato, S. Savasta, and F. Nori, Ultrastrong coupling between light and matter, Nat. Rev. Phys. **1**, 19 (2019).
[65] F. Yan, P. Krantz, Y. Sung, M. Kjaergaard, D. L. Campbell, T. P. Orlando, S. Gustavsson, and W. D. Oliver, Tunable coupling scheme for implementing high-fidelity two-qubit gates, Phys. Rev. Appl. **10**, 054062 (2018).
[66] M. Tokieda, Work-minimizing protocols in driven-dissipative quantum systems: An impulse-ansatz approach (2025), arXiv:2511.15084.
[67] S. Meredith, O. Dudgeon, W. Bukalski, A. J. Brash, H. J. D. Miller, T. J. Elliott, and J. Iles-Smith, Efficient optimisation of multi-parameter quantum control protocols for strongly-coupled systems (2026), arXiv:2604.19621.
[68] G. Bhanja, D. Tiwari, and S. Banerjee, Impact of non-Markovian quantum Brownian motion on quantum batteries, Phys. Rev. A **109**, 012224 (2024), arXiv:2308.14572.
[69] H. Wakaura, Data and code for "Spectral origin and decoupling cost of non-Markovian ergotropy revivals in quantum batteries", Zenodo (2026), all versions, doi:10.5281/zenodo.23587285.
[70] N. Lambert, E. Giguère, P. Menczel, B. Li, P. Hopf, G. Suárez, M. Gali, J. Lishman, R. Gadhvi, R. Agarwal, A. Galicia, N. Shammah, P. Nation, J. R. Johansson, S. Ahmed, S. Cross, A. Pitchford, and F. Nori, QuTiP 5: The quantum toolbox in Python, Phys. Rep. **1153**, 1 (2026), arXiv:2412.04705.